UCRL-18536

cy. 2

LIBRARY AND
DOCUMENTS SECTION

EFFECTS OF FINE PRECIPITATES ON CRITICAL CURRENT DENSITIES OF SUPERCONDUCTING NIOBIUM 1% ZIRCONIUM

Masaki Suenaga
(Ph. D. Thesis)

January 1969

TWO-WEEK LOAN COPY

This is a Library Circulating Copy which may be borrowed for two weeks. For a personal retention copy, call Tech. Info. Division, Ext. 5545

LAWRENCE RADIATION LABORATORY
UNIVERSITY of CALIFORNIA BERKELEY

UCRL-18536

DISCLAIMER

This document was prepared as an account of work sponsored by the United States Government. While this document is believed to contain correct information, neither the United States Government nor any agency thereof, nor the Regents of the University of California, nor any of their employees, makes any warranty, express or implied, or assumes any legal responsibility for the accuracy, completeness, or usefulness of any information, apparatus, product, or process disclosed, or represents that its use would not infringe privately owned rights. Reference herein to any specific commercial product, process, or service by its trade name, trademark, manufacturer, or otherwise, does not necessarily constitute or imply its endorsement, recommendation, or favoring by the United States Government or any agency thereof, or the Regents of the University of California. The views and opinions of authors expressed herein do not necessarily state or reflect those of the United States Government or any agency thereof or the Regents of the University of California.

UCRL-18536

UNIVERSITY OF CALIFORNIA

Lawrence Radiation Laboratory
Berkeley, California

AEC Contract No. W-7405-eng-48

EFFECTS OF FINE PRECIPITATES ON CRITICAL CURRENT DENSITIES OF SUPERCONDUCTING NIOBIUM 1% ZIRCONIUM

Masaki Suenaga*
(Ph. D. Thesis)

January 1969

TABLE OF CONTENTS

ABSTRACT

I. INTRODUCTION 1

II. THEORETICAL ASPECTS 3

III. EXPERIMENTAL ASPECTS 13

A. Preparation of Specimen 13

B. Superconducting Properties Measurements 15

C. Metallography 19

D. Precipitate Sizes and Interprecipitate Spacings 31

IV. DISCUSSION 37

V. SUMMARY 44

ACKNOWLEDGEMENT 45

APPENDIX 46

REFERENCES 49

FIGURE CAPTIONS 53

EFFECTS OF FINE PRECIPITATES ON CRITICAL CURRENT DENSITIES OF SUPERCONDUCTING NIOBIUM 1% ZIRCONIUM

Masaki Suenaga

Inorganic Materials Research Division, Lawrence Radiation Laboratory
Department of Material Science and Engineering, College of Engineering
University of California, Berkeley, California

ABSTRACT

A simple model for flux pinning by non-superconducting precipitates was developed and was compared with the experimental results on Nb 1% Zr alloy. The model predicted that critical current densities, J_c, were approximately proportional to

$$\left(\frac{b}{\delta}\right)^{3/2} \left(\frac{\mathcal{G}}{2\kappa^2 - 1}\right)^{1/2} \left(\frac{H_{c_2} - H}{H}\right) \quad \text{for } b \ll \delta$$

where 2b is the diameter of precipitate, 2δ is the interparticle spacing is the energy of a flux line, κ is the Landau-Ginzburg constant, H_{c_2} is the upper critical field of the alloys, and H is the applied field.

The magnetic field dependence of J_c was in good agreement with experimental results in the cases of intermediate pinning strength. But, for very weak or strong pinning strength, departure of experimental and theoretical results was noted at higher fields. Although it was very difficult to determine exact slopes of a plot

$$\ln \left[J_c/(b)^{3/2}\right] \text{ vs } \ln \delta$$

due to experimental scatter in measured b and δ, the size and the spacing dependence of J_c was thought to be reasonably consistent with the experimental results in spite of simplifying assumptions used in the model.

For measurements of b and δ of precipitates, ZrO_2, a carbon extraction replica method was employed. Transmission electron and optical microscopies were also used to investigate the precipitates.

H_{c_2} (4.2°K) and J_c were measured with use of a superconducting magnet. Critical temperatures, T_c of the alloys were also measured, and it was found that T_c, 9.3°K, varied less than 0.2°K with heat treatments.

I. INTRODUCTION

In type II superconductors, magnetic fields penetrate in a form of a quantized flux lattice when the applied field, H, exceeds the lower critical field, H_{c_1}.[1,2] In a homogeneous superconductor, the flux lines are forced to move because of the Lorentz force. Flux movement produces a voltage drop across a sample when a transport current, which is not parallel to H, is present.[3] It is well known that the motion of flux lines can be prevented or retarded to much higher current densities when crystal lattice defects, such as dislocations and precipitates, are present to pin flux lines.[3,4] Numerous papers have been published on the qualitative relationship between the critical current densities and the nature of defects in superconductors,[4-16] but practically no quantitative investigation of the subject have been reported.[4] This is partly due to the very complicated defect structures of the materials that have been investigated, and to the absence of a simple theoretical model which can be applied to complicated systems (except in the case of grain boundaries at the normal and superconducting material[16]). In the present investigation, a simple model for flux pinning by non-superconducting precipitates was developed and the model was compared with the experimental results of Nb 1% Zr alloy. The model developed is very similar to Orowan's theory[17,18] of the yield strengths of metals containing non-deformable precipitated particles. Since Orowan's theory has been very successful in spite of its simplicity, and because there is a great deal of similarity between dislocations and flux lines, as has been pointed out by Goodman and Matricon,[19] a similar pinning mechanism approach was employed to treat the variation of critical current densities with precipitate size and spacing.

For an investigation of this type, it is desirable that the alloy to be studied forms very fine homogeneously distributed precipitates whose sizes and spacings can be varied with suitable heat treatments. It is also desirable to retain nearly constant superconducting properties such as critical temperatures, T_c, and critical fields, H_{c_2}, for all conditions of heat treatment. With these considerations in mind, an alloy system, Nb-1% Zr plus oxygen, has been chosen. A precipitate, ZrO_2, was formed by internal oxidation. Homogeneous nucleation of ZrO_2 occurs in this alloy.[20,21] According to De Sorbo[22], interstitial oxygen in solution decreases T_c more than any other gaseous impurity (T_c decreasing by 0.93°K per at. % oxygen). To maintain critical temperature variation within 0.5°K, the oxygen content must be kept below 1000 ppm.

Although changes in H_{c_2} with heat treatments cannot be avoided, it is likely that the variation will not be very large since well annealled Nb-1% Zr plus oxygen is expected to be a relatively low κ material where κ is the Ginzburg-Landau constant. H_{c_2} is proportional to κ. The total κ is a sum of two terms, κ_o and κ_ℓ, where κ_o is the Ginzburg-Landau constant which depends on the intrinsic properties of the alloy such as critical temperature and the coefficient of electronic specific heat per unit volume γ, and where κ_ℓ is the Ginzburg-Landau constant which depends on γ and the normal resistivity, ρ_n. If κ_o is comparable with κ_ℓ, the variation of ρ_n with heat treatments will not change κ appreciably. Hence, H_{c_2} should vary but little with aging treatments. With small structural and superconducting parameter variations, the analysis of experimental results is greatly simplified.

II. THEORETICAL ASPECTS

In this section, a model for a flux pinning mechanism by dispersed non-superconducting precipitates in a type II superconductor is considered. The model is intended to show the functional relationship of the critical current densities, $J_c(H)$, to the interprecipitate spacing and precipitate size. The model is similar in form to that used for the pinning of dislocations in crystals by precipitates.[17,18] The similarities between magnetic flux lines in a type II superconductor and dislocations in a crystal are striking.[19]

The main assumptions of this analysis are:

1) Applied magnetic fields, H, are in a region where the density of flux lines is low enough so that the long range interaction between flux lines is relatively weak in comparison with the flux line precipitate interaction.

2) The number of pinning centers per unit area, n_p, is approximately equal to or larger than the number of flux lines per unit area, n_ϕ.

Using these assumptions, one can consider the interaction between a single flux line and precipitates in a Lorentz force field in determining an expression for critical current density. In the following we shall first treat the effect of interprecipitate spacings on critical current density. The precipitate volume effect is then considered.

Consider a type II superconductor in a magnetic field, $H > H_{c1}$, and a transport current density, J. The direction of J is perpendicular to H as shown in Fig. 1a. In such a case, there exists a Lorentz force on flux lines. A general form of Lorentz force can be expressed as:[24,25]

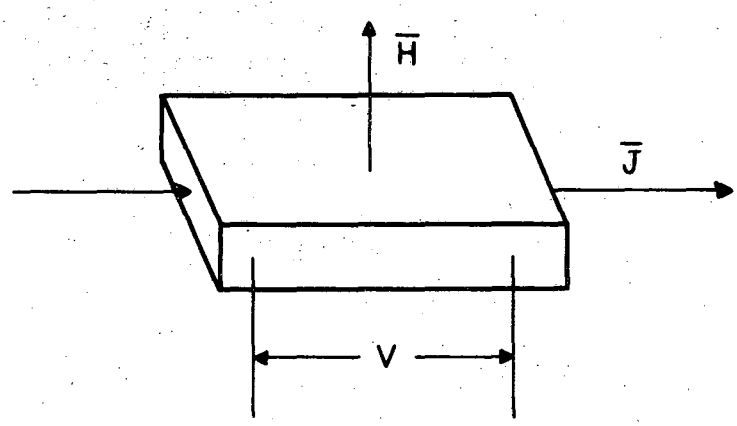

(a)

Fig. 1a A diagram showing the respective orientation of magnetic fields and currents thru a specimen.

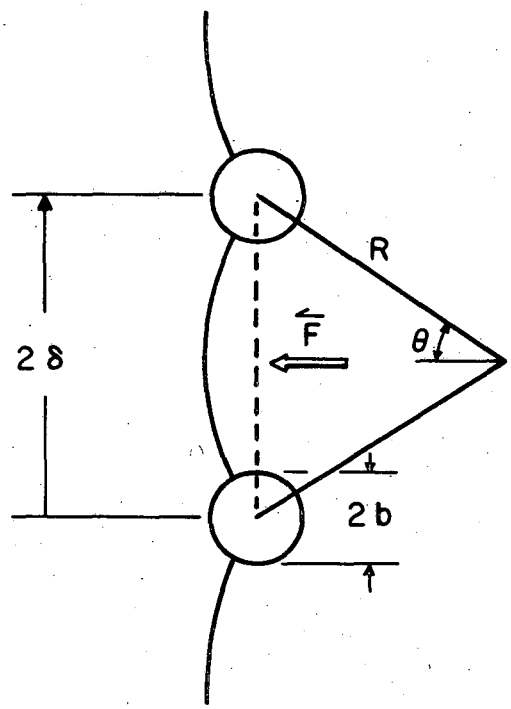

(b)

Fig. 1b A schematic diagram of a flux line which is pinned by precipitates.

XBL6811-7129

$$\vec{F} = \frac{1}{4\pi} \vec{B} \times \text{curl } \vec{H} (\vec{B}) \qquad (1)$$

Unless there are flux pinning centers in the superconductor, the lines will be moved in the direction according to $\vec{F}$. When there are crystal structural defects such as dislocations and precipitates in the superconductor, the potential energy of a flux line varies in the area of the defects. Thus, in the presence of such defects the motion of flux lines is retarded and the flux lines are in equilibrium for a current up to a value such that

$$\frac{1}{4\pi} \vec{B} \times \text{curl } \vec{H} (\vec{B}) - \vec{P} = 0 \qquad (2)$$

where $\vec{P}$ is the total pinning force per unit volume. Here it is assumed that there is no temperature gradient in the region of interest. With the assumptions which have been stated before and with a definition of a transport current density, $\vec{J} = c/4\pi \text{ curl } \vec{H} (\vec{B})$, Eq. (2) can be simplified as

$$\frac{1}{c} \Phi_0 \quad J - p = 0 \qquad (3)$$

where p is the pinning force per unit length, Φ_0 is the flux quantum, 2×10^{-7} g-cm^2, and $\vec{H} \perp \vec{J}$ is assumed. In this simplification we only consider the force on a "single" line instead of a force on a lattice of lines.

The critical value of J for which the Lorentz force exceeds the pinning force is designated as the critical current density, $J_c(H)$, in an applied magnetic field, H. In experimental measurements of $J_c(H)$, a longitudinal voltage on a specimen is correlated with depinning of flux lines since motion of flux lines creates an electric field perpendicular to the

direction of motion of flux lines.[3]

In order to determine the dependence of J_c on the interprecipitate spacing, 2δ, we consider a flux line pinned by a row of precipitates of a uniform diameter, $2b$. As J increases, the pinned lines will increasingly bow out between two neighboring precipitates. (A schematic diagram of the line under Lorentz force is shown in Fig. 1b.) Then, the critical condition for flux depinning of Eq. (3) can be rewritten in terms of the following: Lorentz force, the distance which a segment of a line is moved, Δy, and the pinning energy of precipitates, F_p,

$$\frac{2}{c}\Phi_o J \delta \Delta y - F_p = 0 \qquad (4)$$

The nature and the precipitate size dependence of the pinning energy, F_p, will be discussed later.

Now, the obtaining of $J_c(H)$ in terms of δ and F_p with the use of Eq. (4) and trigonometric relationships shall be considered. The average distance that a segment of a flux line is moved can be expressed as

$$\Delta y = \left[\frac{\delta}{\sin^{-1}\left(\frac{\delta}{R}\right)} - (R^2 - \delta^2)^{1/2} \right]$$

where R is the radius of the curvature as shown in Fig. 1b. Then,

$$J_c(H) = \frac{cF_p}{2\Phi_o \delta} \left[\frac{\delta}{\sin^{-1}\left(\frac{\delta}{R}\right)} - (R^2 - \delta^2)^{1/2} \right]^{-1} \qquad (5)$$

The limiting values of J_c for $\frac{\delta}{R} \cong 1$ and $\frac{\delta}{R} << 1$ can be put as,

$$J_c \cong \left(\frac{\pi}{4}\right)\left(\frac{c}{\Phi_0}\right) \frac{F_p}{\delta^2} \quad \text{for} \quad \frac{\delta}{R} \cong 1 \tag{6a}$$

and

$$J_c \cong \left(\frac{c}{\Phi_0}\right)\left(\frac{F_p}{3}\,\mathcal{J}\right)^{1/2} \frac{1}{\delta^{3/2}} \quad \text{for} \quad \frac{\delta}{R} \ll 1 \tag{6b}$$

where $\mathcal{J}$ is the line energy per unit length of a flux line. $\mathcal{J}$ is approximated as[23,27]

$$\mathcal{J} \cong \left(\frac{3.1}{2\pi}\right) \frac{H_{c_b}^{2}\lambda^2}{\kappa^{1.6}} \quad \text{for } .2 \leq \kappa \leq 10 \tag{7a}$$

and

$$\mathcal{J} \cong \left(\frac{\Phi_0}{4\pi\lambda}\right)^2 \ln\left(\frac{\lambda}{\xi}\right) \quad \text{for } \kappa \gg 1 \tag{7b}$$

In order to obtain Eq. (6b), a relationship, $\mathcal{J}\Delta\delta \cong F_p$, is also used where $\Delta\delta$ is the increase in the length of the line caused by the Lorentz force, $\bar{F}$ from $\mathcal{J} = 0$ condition.

Two limits which have been considered above imply the following in terms of relative energies of F_p and $\mathcal{J}$: the limit, $\frac{\delta}{R} \ll 1$, in the case $F_p \ll \mathcal{J}\delta$ and the limit, $\frac{\delta}{R} \cong 1$, in the case $F_p \cong \mathcal{J}\delta$. Or in terms of relative sizes of δ and b, $\frac{\delta}{R} \ll 1$ and $\frac{\delta}{R} \cong 1$ correspond to $\frac{b}{\delta} \ll 2$ and $\frac{b}{\delta} \geq 2$, respectively. Also, Eqs. (6a,b) suggest that J_c becomes infinite as δ goes to zero, however, a more careful observation points out that the lower limit of δ is the radius of a precipitate, b, by the definition of the interprecipitate separation, δ. Also, in such a limit $\delta \to b$, the argument which has been presented here will not be very valid since the superconducting region of a sample may diminish as $\delta \to b$.

It is interesting to compare these results with other published results. Friedel et al.[25] obtained a relationship $J_c \propto \frac{1}{\delta}$ and Coffey in his "modified London Model"[26] showed that $J_c \propto \frac{1}{\delta^2}$ in the limit $n_p \approx n_\Phi$. Although Coffey's method is entirely different from this approach, his result is in accordance with the present result for the limit $\frac{\delta}{R} \approx 1$.

The next task is to approximate $F_p(H)$ which appears in the expression for J_c. The free energy of superconducting electrons in a magnetic field can be expressed as [23]

$$\mathcal{F}_e\ (H) = \int E_e d^3r + E_{kin} + E_{mag} \tag{8}$$

where F_e is the energy of the electrons in a condensed state at rest, E_{kin} the kinetic energy associated with permanent currents, and E_{mag} the magnetic field energy. The basic idea of the origin of the pinning energy F_p, is that the free energy varies depending on how flux lines are positioned with respect to the precipitates. In particular superconducting condensation energy is lost both in the normal cores of the flux lines and in the precipitates so that the energy is minimized by superimposing the flux lines on the precipitates. Also, changes in the magnetic field distribution of flux lines take place when flux lines are moved into or out of the precipitates. This results in a change of $(E_{kin} + E_{mag})$ since E_{kin} and E_{mag} are proportional to $\int (\nabla \bar{h})^2\ d^2r$ and $\int (\bar{h}^2) d^2r$, respectively. An exact calculation of F_p is a very difficult task; therefore we only consider cases where simplifications are possible.

Suppose that the radius of precipitates, b, is smaller than the superconducting coherence length, ξ. Then the decrease in energy by positioning a flux line at the precipitate is approximately given by

$$F_{p_c} \approx \frac{4}{3}\pi b^3 \, g(H) \tag{9}$$

where g(H) is the free energy of a type II superconductor in magnetic fields, per unit volume. Using Abrikosov's expression[1] for g(H), Eq. (4) becomes

$$F_{p_c} \approx \frac{1}{6} b^3 \frac{(H_{c_2} - H)^2}{1.2\,(2\kappa^2 - 1)} \tag{10}$$

where H_{c_2} is the upper critical field and κ is the Ginzburg-Landau parameter. Strictly speaking, the expression for g(H) is only applicable for $H \approx H_{c_2}$ and for a reversible type II superconductor. We can approximate g(H) for the non-reversible superconductor with that of the reversible one in the absence of more accurate expressions for g(H) non-reversible.

When $\xi \lesssim b$, the contribution to F_p from the magnetic energy terms becomes important. Phenomenologically, one can write the pinning energy as

$$\begin{aligned} F_{p_m} &= \Delta\,(E_{kin} + E_{mag}) \\ &= \Delta\left(\frac{1}{8\pi} \int [h^{-2} + \lambda^2(\nabla \times \bar{h})^2] d^3r\right) \end{aligned} \tag{11}$$

where Δ indicates the difference of the energies, $(E_{kin} + E_{mag})$ with or without a precipitate about the flux line. In order to calculate this energy, F_{p_m}, the magnetic field distributions with and without precipitates about a flux line have to be determined. However, determinations of $\bar{h}(r)$ are again difficult except in a very special case where $\kappa \gg 1$[23] and in a case where no precipitates are present. In other cases the use of computer calculations are required.[26-28] Since it was shown that $F_{p_c} > F_{p_m}$ for $\kappa > 1$[26] and we are interested in the region $\xi \geq b$, we will not proceed with the discussion of F_{p_m} and we assume that $F_p \simeq F_{p_c}$.

Finally, combining the above results critical current densities, J_c, become

$$J_c \cong \frac{c\pi}{24} \frac{b^3}{\Phi_0 \delta^2} \frac{(H_{c_2}-H)^2}{1.2(2\kappa^2-1)} \tag{12a}$$

for $\frac{\delta}{R} \cong 1$ and

$$J_c \cong \frac{c}{\Phi_0 \delta^{3/2}} \left(\frac{8b^3}{3}\right)^{1/2} \frac{\left(H_{c_2}-H\right)}{(1.2)^{1/2}(2\kappa^2-1)^{1/2}} \tag{12b}$$

for $\frac{\delta}{R} \ll 1$.

In the experimental measurements, a voltage which appears between the two ends of a sample is measured and the criterion for J_c will depend on the sensitivity of the voltage detecting system. If a preselected voltage (e.g. 10^{-6} volts/cm) is used as a criterion, the appearance of the voltage may not correspond to the current densities at which all flux lines are depinned from precipitates at all fields. The voltage which is detected between the ends of the sample will depend on the number of flux lines in motion and their velocity. It was expressed by Kim et al.[3] as

$$V = n_\Phi \frac{v_L \Phi_0}{c} \ell = \ell \frac{v_L}{c} B \tag{13}$$

where ℓ is the length of the sample, v_L is the velocity of flux lines, and n_Φ is the number of flux lines per unit area. Assuming that v_L does not vary substantially with n_Φ, the voltage is directly related to the number of flux lines per unit area or the magnetic field strength in a superconductor. Therefore, the experimental value of J_c should be multiplied by a factor proportional to B, or

$$J_{c\ \exp} \sim \frac{m}{B} J_c \tag{14}$$

where m is a multiplicity factor which takes into account that all flux lines would not be released from pinning sites at the same instance.

Finally, critical current densities become

$$J_c \quad \exp \approx \frac{b^3}{\delta^2} \, m \, \frac{(H_{c_2}-H)^2}{H} \quad \frac{1}{(2\kappa^2-1)} \quad \text{for } \frac{\delta}{R} \cong 1 \tag{15a}$$

and

$$J_c \quad \exp \approx \left(\frac{b}{\delta}\right)^{3/2} m \left(\frac{g}{2\kappa^2-1}\right)^{1/2} \frac{H_{c_2}-H}{H} \quad \text{for } \frac{\delta}{R} \ll 1 \tag{15b}$$

In the following sections, experimental results are compared with these relationships.

III. EXPERIMENTAL

A. Material Preparations

The alloy was prepared by melting approximately 15 grams each of swaged high purity Nb rods and cold pressed Nb poweder pellets with 0.3 grams of Zr wire in a cold mold arc furnace under an argon atmosphere. The ingots were turned and remelted several times to enhance homogeneity of the alloy. Then, these ingots were cold-rolled to approximately 30 mils and cut to approximately 2 in. × 3/8 in. pieces for heat treatment.

After the surfaces of alloy sheets were chemically cleaned with 50% HF - 50% HNO_3 at room temperature, they were subjected to homogenization and solution treatments in an "Abar" furnace. The amount of residual gaseous impurity contents in the alloy after heat temperature depended greatly on temperature, vacuum conditions, and the lengths of heat treatment.[29] Therefore, in order to prepare alloys with different oxygen contents, the specimens were solution treated in the following manner: alloy A at 1800°C for 3 hours and 2) alloy B, at 1900°C for 1-1/2 hours*. The chemical analysis of these alloys and starting materials were made by

---

*Temperatures were determined with the use of an optical pyrometer. Since the accuracy of the temperature measurements by an optical pyrometer at high temperatures becomes somewhat poor,[30] the pyrometer reading was compared with the melting point of a pure platinum wire. It was found that the pyrometric reading was approximately 40 degrees higher than the melting point of Pt (T_m = 1769°C). Hence, the homogenizing temperature which were used could be as low as 1860°C and 1760°C instead of 1800°C and 1900°C, respectively.

Anamet Laboratories, Inc. and are given in Table I.

After the solution treatments were completed, the alloys were quenched in a diffusion pump oil bath. This resulted in the formation of the thick black Nb-carbide layers on surfaces of the samples. The layers were so hard that surface grinding with metallurgical polishing papers was necessary in order to remove the layers. During polishing, special care was taken to prevent any bulk deformation of samples. Before further heat treatments each sample was chemically polished in a solution of 40% HF + 60% HNO_3 at 0°C. Chemical polish accomplished two purposes. One was surface cleaning and the other was the removal of deformed surface materials that produced by the grinding process.

In order to form the desired precipitates, pieces of the homogenized alloys were encapsulated in quartz tubings at approximately 100 Torr of purified argon, and heated at 1000°C in a platinum resistance heating furnace for specified periods. According to the phase diagram showing the solubility of oxygen in Nb 1% Zr alloy, [31,32] ZrO_2 precipitate was expected to form during this heat treatment. After specified heating periods, the quartz tubes were quenched into ice water and the tubing was then broken.

Specimens for superconducting property measurements were spark cut in order to avoid deformation of samples. However, a thin layer of Nb carbide formed on the surfaces of the alloy during spark cutting. Thus it was necessary to electro-polish the surface of the alloy before testing for superconducting properties. Samples for the critical current densities and critical fields measurements had cross sections of approximately 20 mils × 15 mils.

Specimens for optical microscopy and replication electron microscopy

TABLE I.

Chemical Analysis of Starting Material and Alloys (ppm)

	$Nb_{(rod)}$	$Nb_{(powder)}$	Alloy A	Alloy B
C	20	650	17	20
N	60	670	50	12
O	60	1000	330	70-100
Fe	<50	480		
Mo	<20			
Ta	830	1400		
W	<100			
Zr	<100		10^4	10^4

were taken from the same specimen used for J_c and H_{c_2} measurements.

For transmission electron microscopy, a special set of specimens, approximately 6 mils thick was prepared. After being homogenized, instead of cooling by quenching into the diffusion pump oil baths, they were rapidly cooled by introducing cold argon into the furnace. By the use of this cooling method, it was possible to use thin foil (~ 6 mils) specimens which make specimen preparation for transmission electron microscopy easier. These samples were then heat treated as described above. Electropolishing of the foils was carried out in a solution (600 ml Methyl Alcohol, 30 ml H_2SO_4 and 15 ml HF) at approximately -60°C. The voltage used was between 25 to 40 volts, depending on the samples and the exact temperature of the solution.

B. Superconducting Properties Measurements

Superconducting critical temperatures were measured by observing changes in impedance of a copper wound coil in which the sample was placed. All measurements were carried out using 1 kHz. In principle the method employed was similar to that of Merriam and von Herzen.[32] The signal from the coil was plotted on one of the axes of an x-y recorder. The signal from a calibrated germanium resistance thermometer was plotted on the other axis. The accuracy of the thermistor was ± 0.1°K. The results of the T_c measurements are tabulated in Table II. To indicate width of the transition, the on-set and the completion of the transition as well as the half inductance temperatures are shown. The half inductance temperature was taken as the critical temperature for superconducting parameters calculations.

TABLE II.

Superconducting Properties of Alloys

	heat treatments	critical temperatures T_c °K	critical field H_{c_2} (4.2°K) kG	Normal State Resistivity ρ_n μ ohm-cm
ALLOY A	As quenched	9.0_8-9.1_8-9.4_2	5.2_0	1.84
	1.0 hrs	9.0_8-9.2_5-9.4_2	5.0	1.54
	2.5 hrs.	9.1_6-9.3_1-9.4_3	4.6_5	1.15
	1.0 hrs.	9.2_5-9.3_9-9.5_2	4.6_5	1.16
	10. hrs.	9.2_5-9.3_3-9.4_3	4.5	1.05
	27. hrs.	9.2_0-9.3_3-9.6_2	4.5	9.82
ALLOY B	As quenched	9.1_6-9.2_2-9.4_8	5.0_5	1.98
	10 hrs.	9.1_6-9.2_5-9.4_8	5.0_0	1.79
	17 hrs.	9.2_5-9.3_3-9.5_7	4.8_2	1.50
	25 hrs	9.1_2-9.2_7-9-4_3	4.8	1.29
	50 hrs	9.1_2-9.2_6-9.4_8	4.7_5	1.27
	100 hrs	9.1_6-9.3_0-9.5_2	4.6_5	1.20

The result of critical temperatures were in accordance with our expectations. The T_c of the quenched samples for alloys A and B were very close to that of pure Nb. Due to purification of the matrix by internal oxidation forming ZrO_2 and other oxides,* increased very slightly (about 0.1°K) with increased aging time. Some Zr remained in solution after all of the oxygen was used up in forming ZrO_2. This made the T_c of the alloy slightly higher than that of Nb. The width of the normal to superconducting state transition was between 0.3°K and 0.4°K, indicating that alloys were homogeneous.

In measuring critical fields (4.2°K) and critical current densities, a standard four-contact resistance probe method was used. The distance between the voltage contacts was 1 in. The magnetic fields were supplied by a superconducting magnet made from Nb-Zr wire. Currents were supplied by a transitor-operated direct current supply which was capable of supplying up to 150 amps. In order to avoid destruction of specimens at high current densities after the transition had taken place, a preselected voltage ($\sim 10^{-5}$ volts) across the specimen was fed back to the current supply so that the supply could be shut off before appreciable heating of the specimen could occur. However, at very high current densities ($J > 5 \times 10^4$ A/cm^2), the delay time for the current shut off was not always short enough to avoid melting of the specimen.

The results of the measurements of J_c and H_{c2} are shown in Fig. 2. For simplicity only representative results are plotted. Some specimens of

---

*Identification of precipitates will be discussed in the next section.

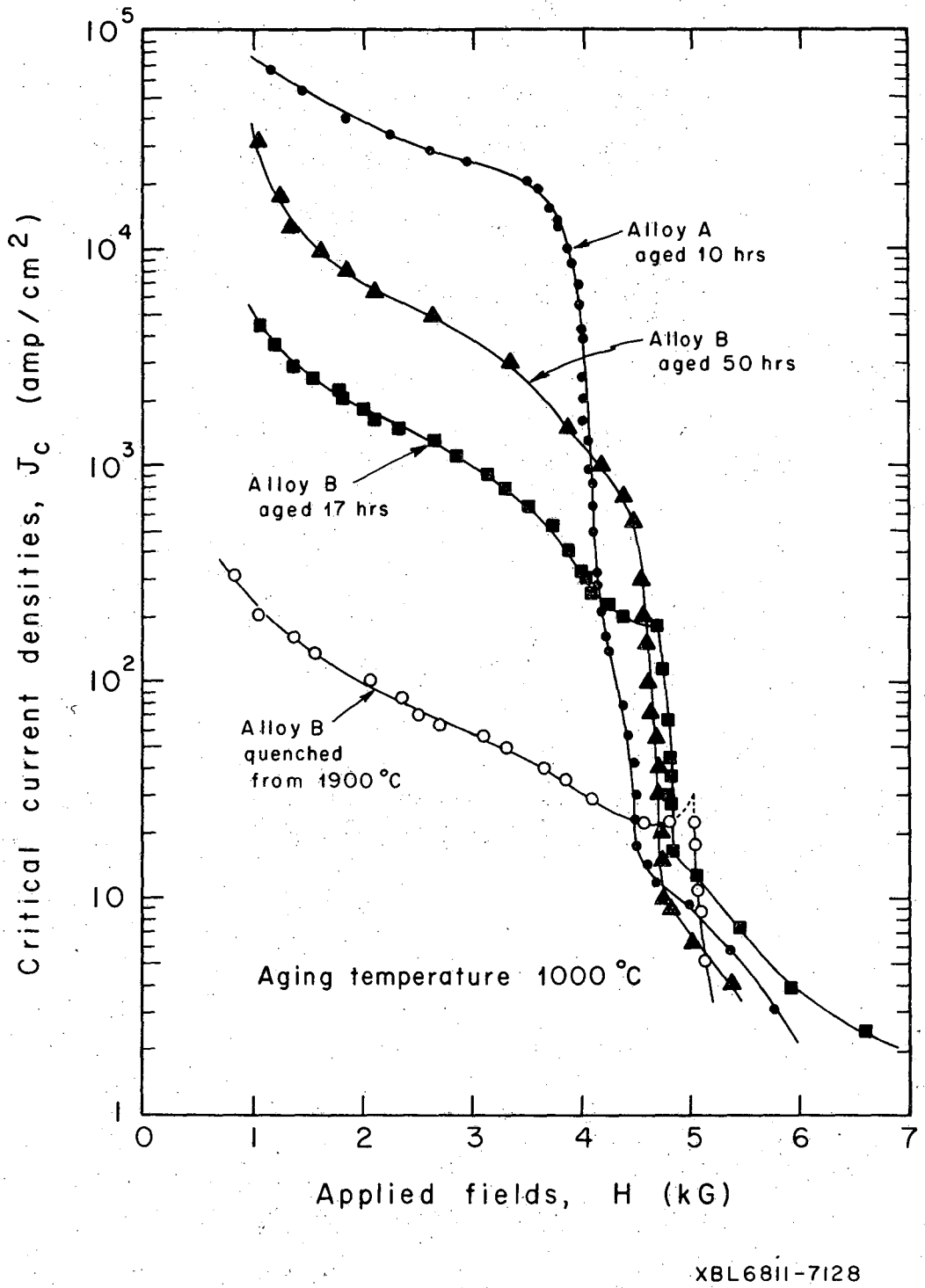

XBL6811-7128

Fig. 2. Plots of critical current densities vs. applied fields for the alloys A and B.

alloy B which were quenched and aged for short periods exhibited "peak - effect" for which the mechanism is not yet completely understood. With increasing aging time critical currents increased and the peak effect disappeared. Aging of specimens for more than 100 hours was not attempted because an oxygen pick up was noticed for longer treatments at 1000°C.

Critical fields values were taken as the field where J_c decreased very rapidly for a small increase in applied field. It was also possible to determine H_{c_2} from very low current resistive transition as the applied field was swept over the transition field. However, this method was hampered by the fact that there was an appreciable amount of surface superconductivity below 10 amp/cm^2 making it very difficult to determine consistent H_{c_2} values. The values H_{c_2} for all specimens are included in Table II. The variation of critical fields with heat treatments was approximately 0.5 kG which is approximately 10% of H_{c_2}. Also, the variation of H_{c_2} with the normal state resistivity is in accordance with GLAG theory.[1,34,35]

A specimen was tested before and after being electropolished since there was a question in pinning flux lines by rough surfaces. However, it was found that surface pinning of flux limes was negligible compared with bulk pinning.

C. Metallography

1. Optical microscopy

All specimens were electropolished in a solution, (300 ml, methyl alcohol 15 ml H_2SO_4, 7.5 ml HF) at a temperature of .50°C. Electropolishing proved to be necessary to avoid surface damages from mechanical

polishing. This was especially true for those specimens which were not heat treated for a long period to produce an appreciable amount of precipitate. After electro-polishing, specimens were chemically etched in an aqueous solution of HF - HNO_3 - H_2SO_4 between 30 sec and 1-1/2 min. depending on the thermal history of the specimen.

The sequence of events during aging of alloys are shown in Fig. 3. The presence of some undissolved precipitates observable in the alloy A indicated that the homogenization process was not fully completed. However, the alloy B was completely homogenized and no precipitates were detectable in the unaged specimen. During the initial stage of aging (1 hour for alloy and 10 hours for alloy B at 1000°C) very small precipitates started to appear. Then a very dense precipitate appearance was observed with further heat treatments. With an optical microscope variation in precipitates in size and density was not very clearly seen after the initial stage except in the alloy B heated for 100 hours which indicated coarsening of precipitates. As observed by Barber and Morton[32], segregation of precipitate and recrystallization in some areas were also observed in the alloy. Also, a very large difference in grain sizes between the alloys A and B are observed. This is due to the difference in homogenizing temperatures.

2. Electron Microscopy

There are two experimental methods that can be used in determining precipitate sizes and densities. These are transmission electron microscopy either by foils or replication, and scanning electron microscopy. The guaranteed resolution of a scanning electron microscope is approximately 250Å.[36] This method was not used in our investigation because the size of precipitates were expected to be in a range of 50Å - 1000Å.

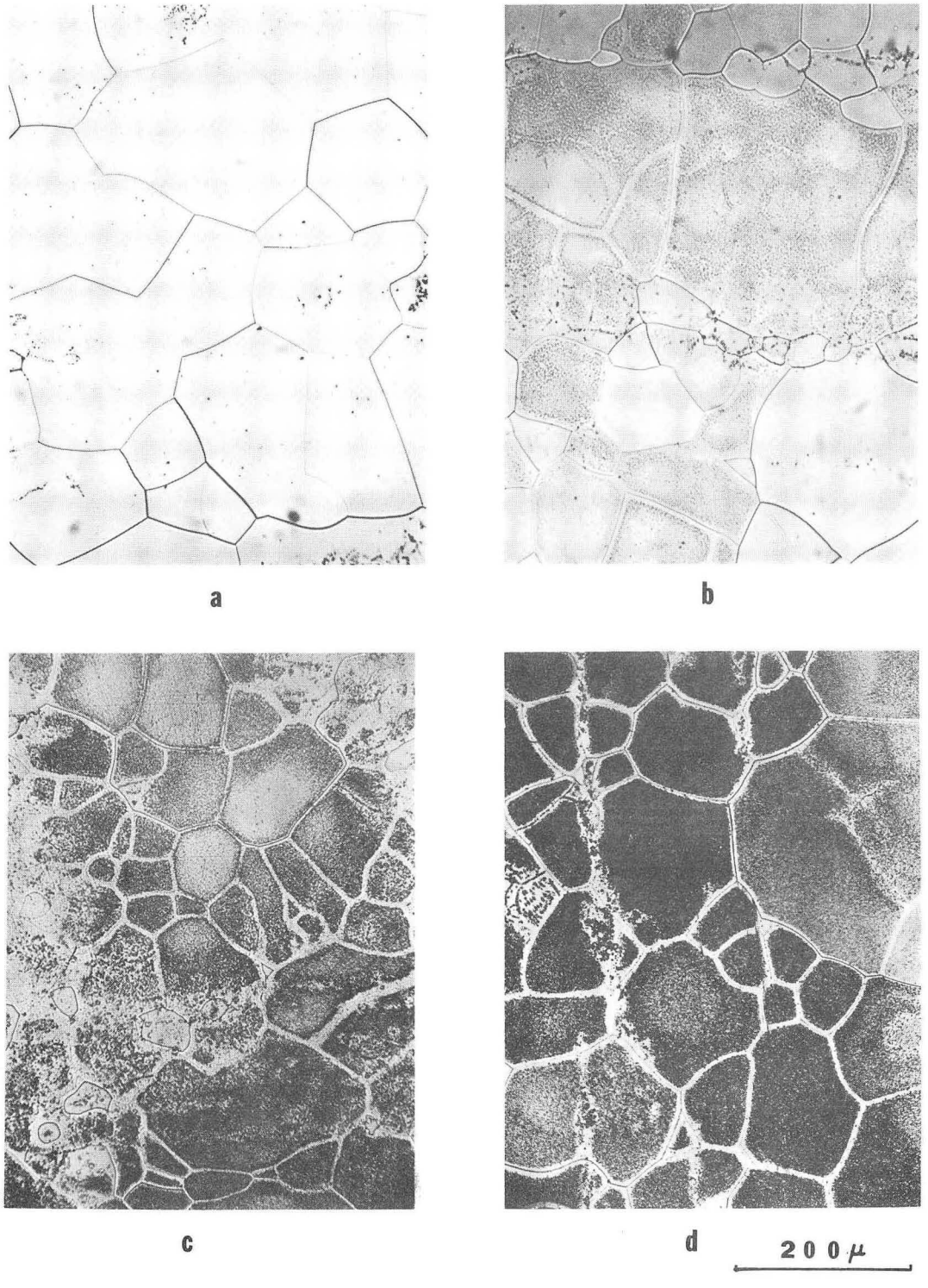

XBB 6811-6833

Fig. 3a. Optical micrographs of the alloys A. (a) as quenched from 1800°C, and aged at 1000°C for (b) 1 hour, (c) 10 hours, and (d) 27 hours.

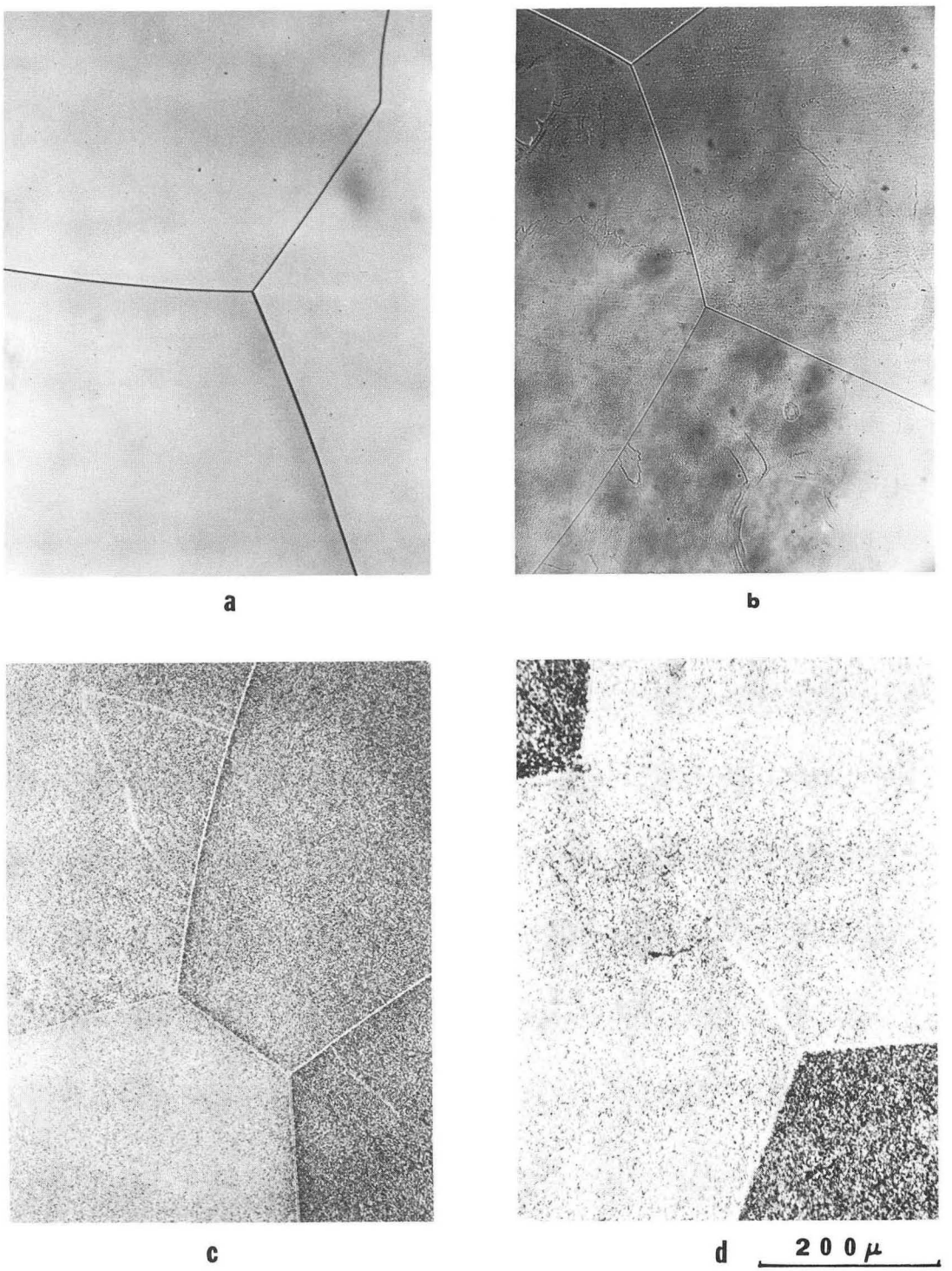

XBB 6811-6837

Fig. 3b. Optical micrographs of the alloys B. (a) as quenched from 1800°C, and aged at 1000°C for (b) 10 hours, and (c) 25 hours, and (d) 100 hours.

Although the interpretation of the projected images of precipitates in a thin foil by transmission electron microscopy is difficult, there is generally more information available on the nature of the precipitates by transmission electron microscopy than by the two dimensional measuring methods[37], such as replication microscopy. A considerable amount of effort was expended in determination of the sizes and densities of precipitates by means of transmission electron microscopy. However, in this method we encountered a major difficulty in the measurement of the foil thickness which is necessary in determining the distribution of the precipitates. Among several possible methods available[37] for the thickness measurement, the slip trace analysis was considered to be the best method for our purpose. But it was almost impossible to obtain consistent thickness measurements due to the multiple slip system in a bcc crystal. Also, when there are densely placed precipitates in a foil, it is again almost impossible for dislocations to move freely so that slip traces become observable.

Although very few quantitative measurements were made on the precipitates by transmission electron microscopy, the information that was obtained is valuable. Micrographs for different heat treatments are shown in Fig. 4. We note that the densities and the sizes of precipitates increased with aging time. In some cases precipitates had grown into elongated rods with increasing aging time. Although it is not obvious in these micrographs, these precipitates were later shown by replication microscopy to be cubes or rectangular rods. It was also observed that very few dislocations were present. Hence, we can conclude that pinning of flux lines was solely due to the presence of precipitates.

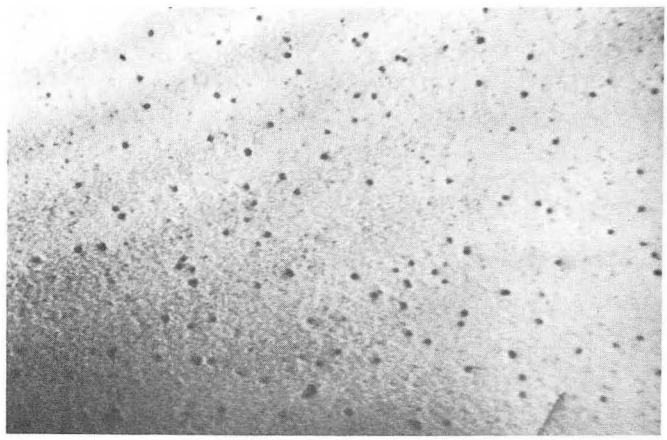

a

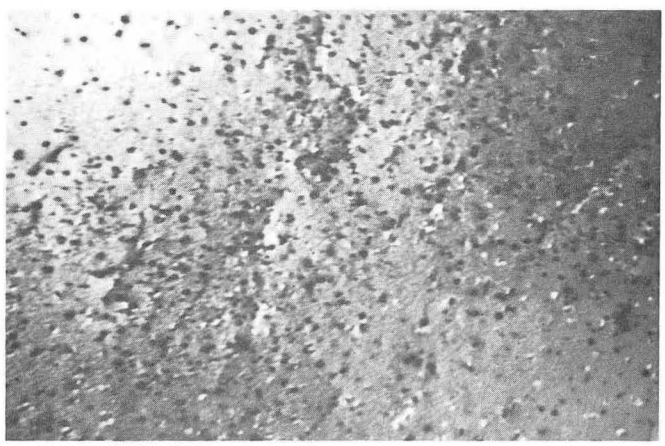

b

c 1 μ

XBB 6811-6834

Fig. 4. Transmission electron micrographs of the alloys Nb 1% Zr. (a) as quenched from 1900°C then aged at 1000°C for (b) 10 hours and (c) 35 hours.

With surface replication electron microscopy, the information which obtained is two dimensional (surface projection), in contrast to the transmission electron-microscopy ("bulk" projection). Hence, the interpretation of micrographs in measuring sizes and distributions of precipitates is greatly simplified. However, there are disadvantages in the use of the ordinary replica method in comparison with the transmission method in areas of lower resolution,* in areas of possible unfaithful replication of a real surface, and in areas of unsuitable specimen condition for electron diffraction.[38,39] In addition, because a replica is a substitute for an actual surface, the occurrence of artifacts is more prevasive, and their recognition is very important in the interpretation of an electron micrograph. Furthermore, the preparation of surfaces to be replicated requires a painstaking skill in order to obtain consistent quantitative measurements of very fine precipitates. However, with the use of the carbon "extraction" replica method,[41] which is extensively used for investigation of precipitates in ferrous metals, many of the difficulties can be avoided. The method consists of evaporation of carbon film on a surface, a preferential etching of a matrix and an adhesion of precipitates on a carbon film. Because precipitates on the surface of the film are directly observed by the microscope, the resolution of electron micrographs become much better than an ordinary direct carbon replica. The accuracy in size measurements is greatly enhanced.

---

*The useful range of sizes of the topographical details imaged is from about 3μ down to about 100Å.

For this reason, we have employed the extraction replica method to measure sizes and distribution of the precipitates in Nb. It was also possible in our experiment to measure precipitates to 50 Å or less with very little error.

Figure 5 shows representative electron micrographs of alloys A and B. Variation in sizes and distributions of precipitates with aging time and contents of oxygen is clearly shown. Apparently the quenching rate which was employed was not rapid enough to completely retain Zr and oxygen in solid solution, and very small precipitates (less than 30 Å - 50 Å) were observed in some areas. Precipitates were mostly cubic, but some of them were rectangular in shape when longer aging times were used.

In the optical microscope scale, precipitates were very uniformly distributed in the alloys B and also in the alloys A as shown in Fig. 3. However, the sizes and distributions are not as uniform as one would like to have in the electron microscope scale. An example of how the sizes and the distributions appear at different magnifications are shown in Fig. 6.

Confirmation of precipitates as tetragonal ZrO_2, a high temperature phase of ZrO_2, was made by analyzing electron diffraction rings, such as those shown in Fig. 6(d). When the precipitates were very small in size or low in number, the intensity of the rings was very weak, and measurements of lattice spacing ratios were difficult in such cases. The results of studying the ring patterns indicated that at early stages of the aging process only tetragonal ZrO_2 lines were observed. Some weaker, possibly NbO_2[42] lines in addition to the tetragonal ZrO_2 lines, begin to appear as the aging was extended. No attempt was made to complete identification of phases possibly present such as Nb_2O_5 - $6ZrO_5$ and ZrC[32] since these phases are

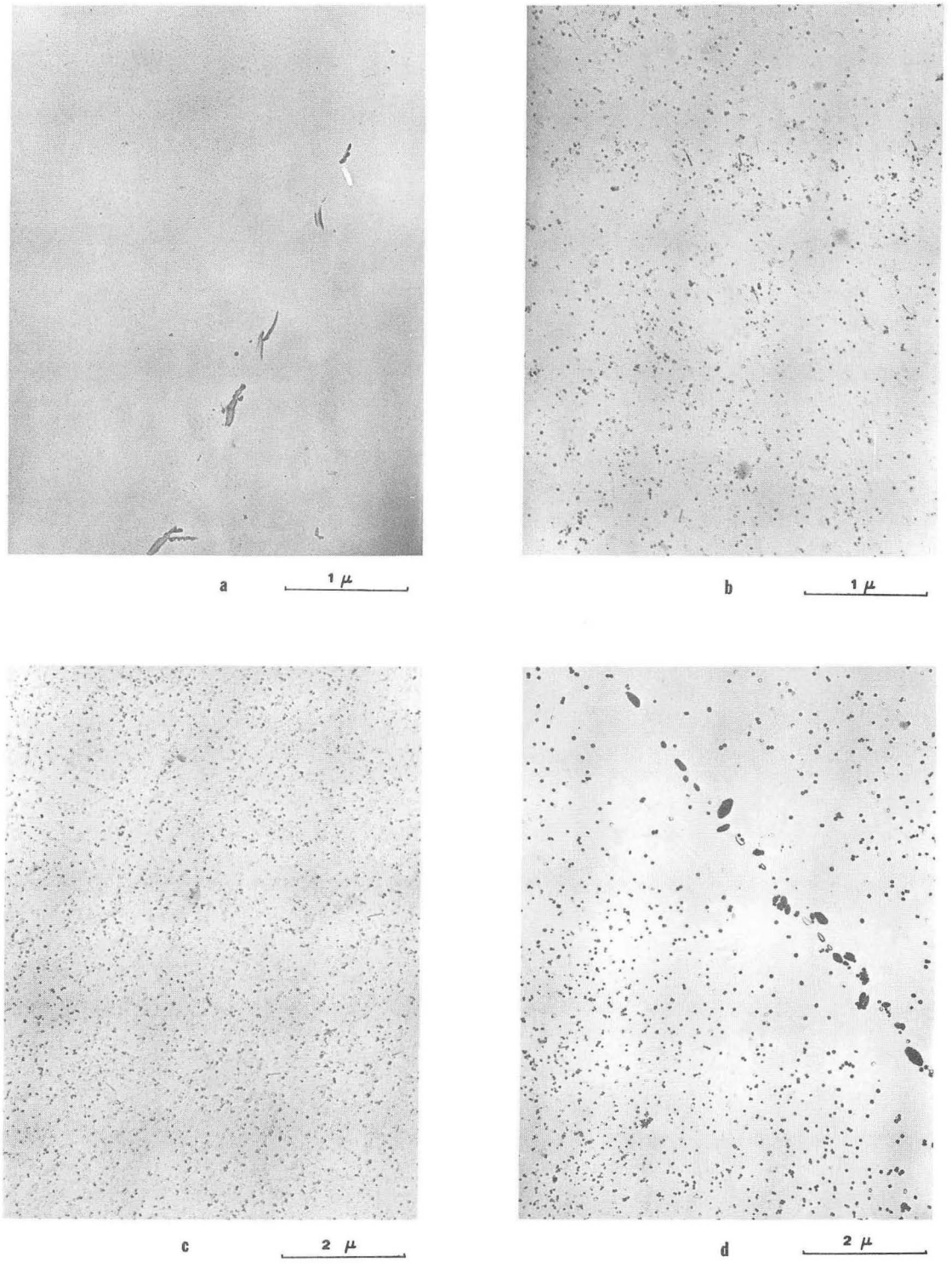

XBB 6811-6835

Fig. 5a. Carbon replication micrographs of the alloys A. (a) as quenched from 1800°C, and aged at 1000°C (b) 2 hours, (c) 10 hours, and (d) 27 hours.

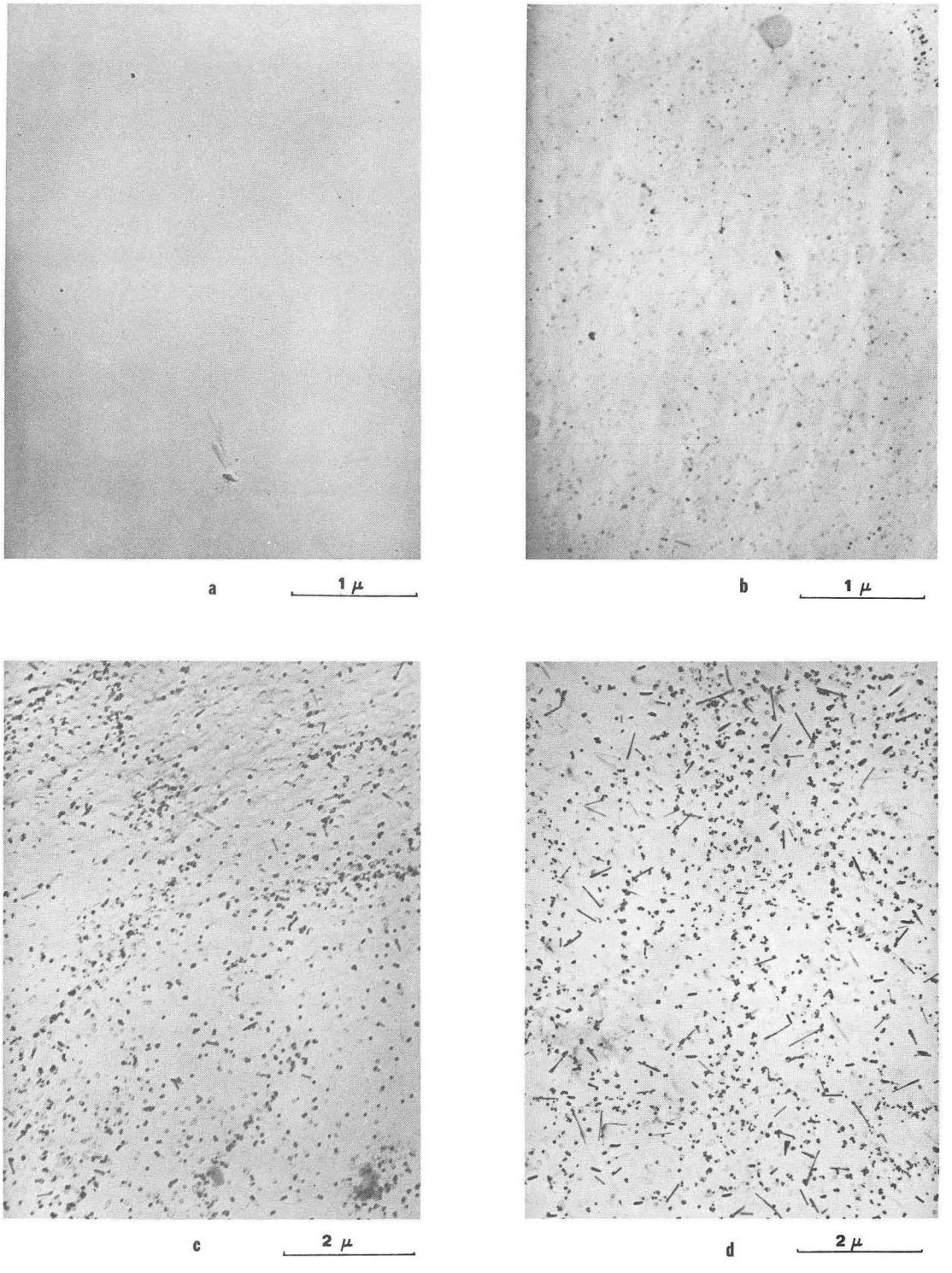

XBB 6811-6838

Fig. 5b. Carbon replication micrographs of the alloys B. (a) as quenched from 1900°C, and aged at 1000°C for (b) 10 hours, (c) 25 hours, and (d) 50 hours.

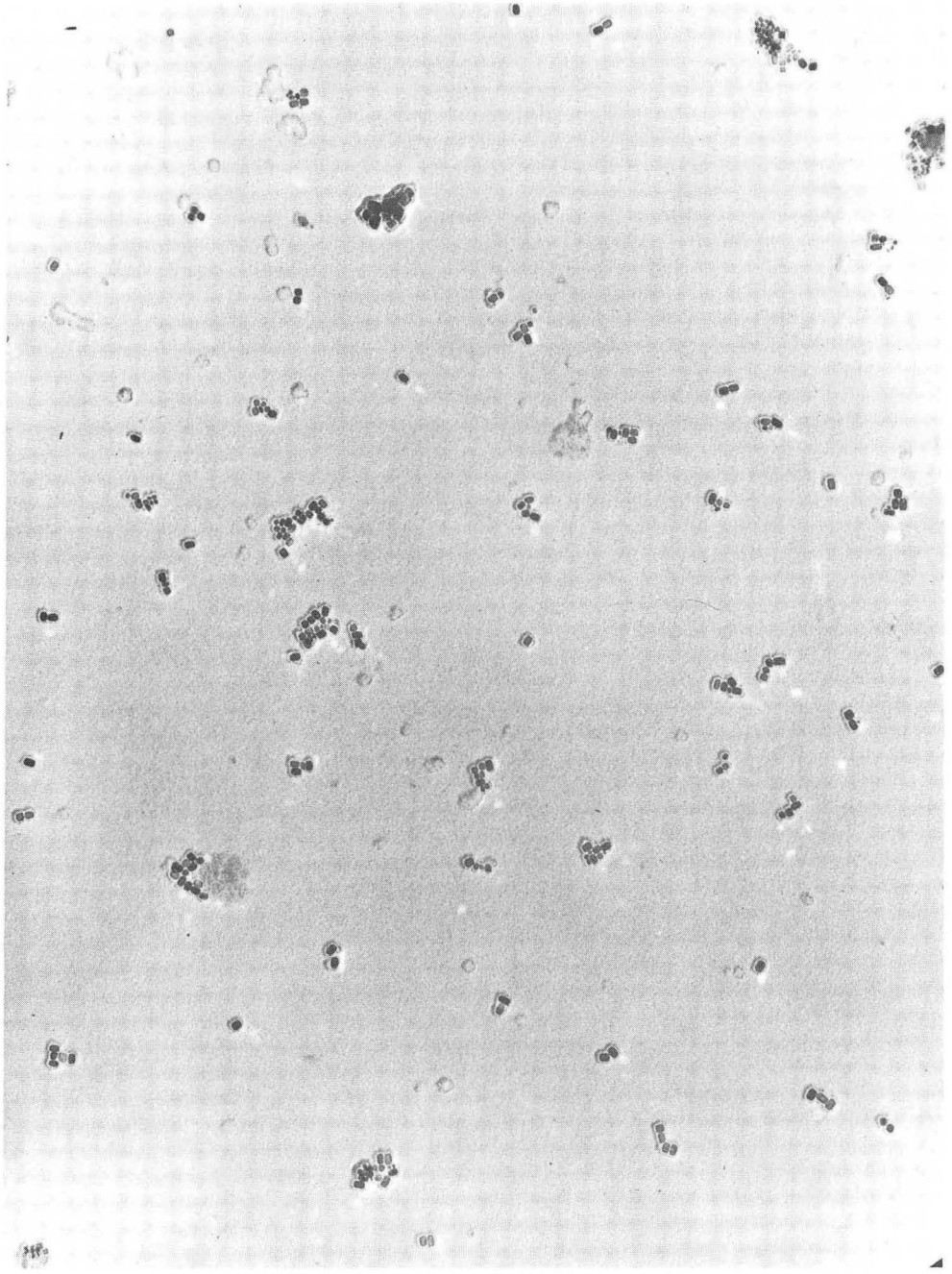

0.5 μ

XBB 6811-6831

Fig. 5c. Carbon replication micrograph of the alloy A quenched from 1800°C and aged from 1 hour at 1000°C showing details of the precipitates.

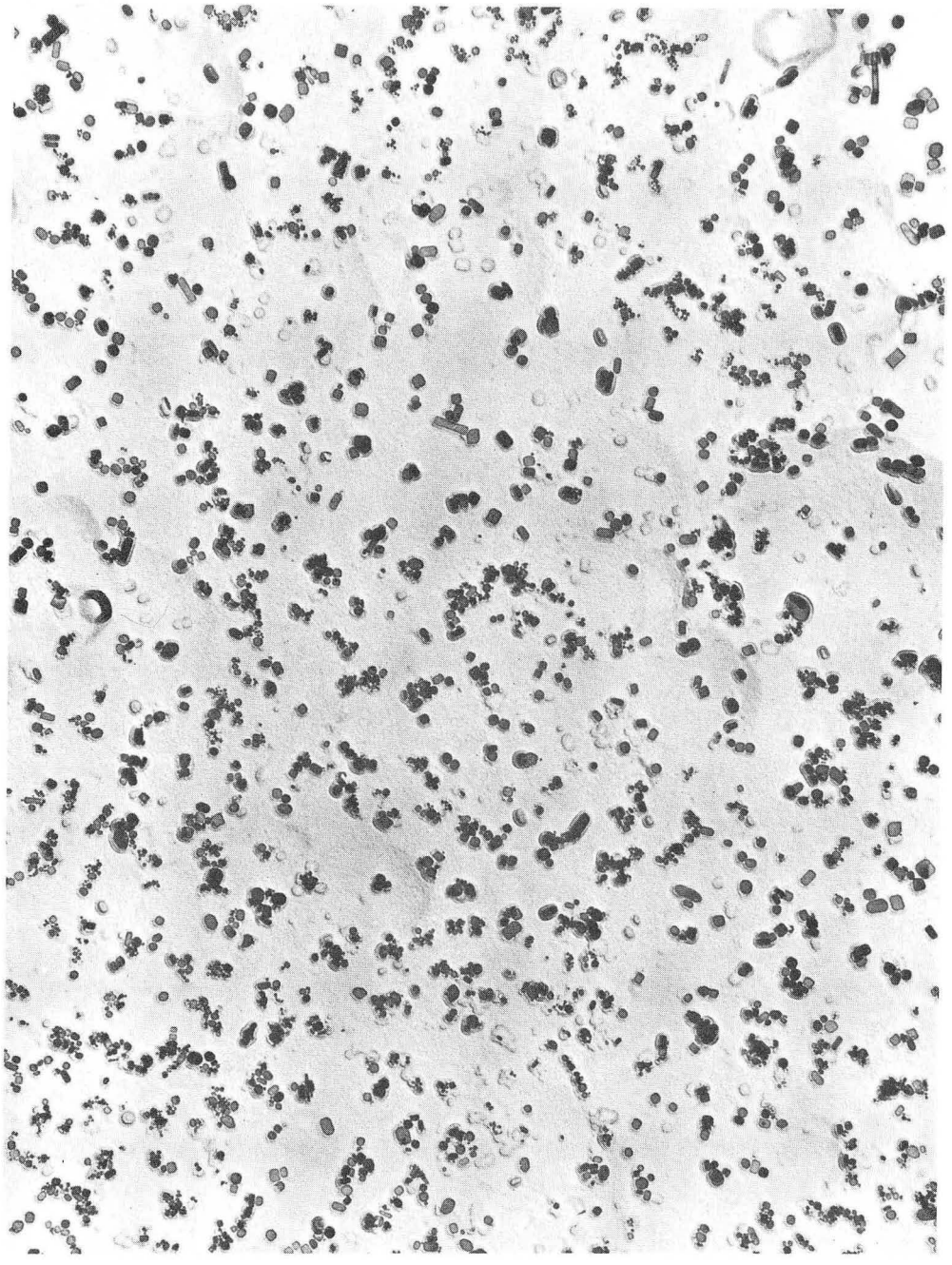

1 μ

XBB 6811-6832

Fig. 5d. Carbon replication micrograph of the alloy A quenched from 1800°C and aged for 27 hours showing details of precipitates.

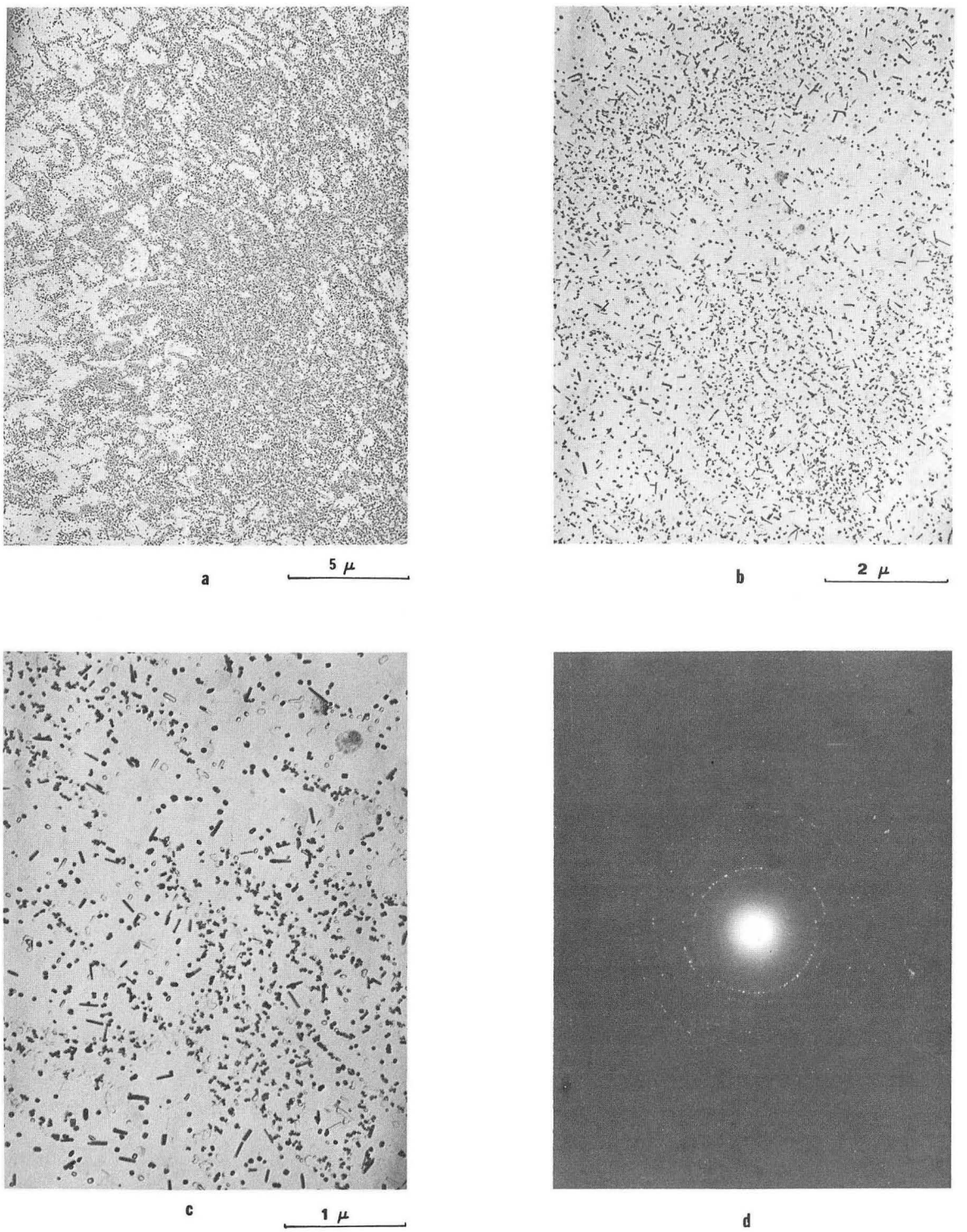

XBB 6811-6836

Fig. 6. The alloy B aged at 1000°C for 50 hours. An example of replication micrographs showing variations of precipitated distributions which are observed at different magnifications, and an electron diffraction rings from the area shown.

most likely non-superconducting and the pinning of flux lines by these possible phases should not change from the pinning by ZrO_2.

D. Precipitates Size and Spacing Measurements

1. Determination of Average Sizes, 2b

There are several published discussions [43-45] on comprehensive method of determining particle size distributions in opaque bodies from a polished cross section. However, these methods are not applicable to size determination of particles from extraction replica data since an extracted surface does not represent a smooth polished cross section. Hence, we have taken a simple but reasonable approach in determining average precipitate sizes, i.e. we assumed that a precipitate which was observed in micrographs such as shown in Figs. 5 and 6 did not represent a part of the precipitate. Such a problem arises in the case of picture taken from a smooth polished cross section since the surface may only cut a very small part of a precipitate which consequently may be observed as a small particle. The advantages of an extraction replica method is that the entire precipitate is seen instead of a part of it. Hence, observed precipitates on the micrographs represent true sizes in bulk. If we assume that there is no preferential extraction of precipitates with respect to sizes of precipitates, then particles observed in the micrographs truly represent all those in a bulk specimen. This assumption seems to be well justified by comparing the sizes of extracted precipitates and the sizes of precipitates which were not extracted. Unextracted precipitates were observed in the micrographs because they produced carbon film thickness contrast. However when precipitates were very small ($\lesssim$ 100 Å), it was very difficult to extract many precipitates and avoid large etch pits which introduce

difficulties in measuring of precipitates sizes. Only painstaking effort in preparation of replicas can minimize this problem.

Determination of the average sizes of precipitates consists of measuring each precipitates with a measuring magnifier (×7) on micrographs and making histograms. Magnifications which were used were approximately ×68,000 and ×34,000 for small ($\lesssim$ 150 Å) and large($\gtrsim$ 150 Å) average sizes of precipitates respectively. Exact magnifications of each micrographs vary slightly from one to another due to small variation of specimen position in an electron microscope. Calibration of magnification was made by the use of a carbon grating (54,800 line/inch) for each objective lens current setting for constant intermediate and projector current settings. Since the accuracy in measuring with the magnifier is better than ±0.50 mm the accuracy of each reading is approximately ±7Å or ±15Å for the small and large precipitates, respectively. However, for larger, errors which were introduced in magnification calibration, many become larger than ±15Å.

Histograms are made for each specimen and each histogram is a result of more than 400 precipitates measurements. Examples of histograms are shown in Fig. 7 . From such histograms, two types of average sizes were determined. They are defined as $\bar{b} = \frac{\Sigma\, ni\, bi}{\Sigma n_i}$ and $\bar{b}_v = \left(\frac{\Sigma\, n_i\, b_i^3}{\Sigma n_i}\right)^{1/3}$. $\bar{b}_v$ is volume weighed average. The determination of $\bar{b}_v$ was necessary since the pinning strength depends on the volume of precipitates and larger precipitates are more effective than smaller ones in pinning.

Variations of $\bar{b}_v$ with aging time are plotted in Fig.8 $\bar{b}_v$ for the as-quenched specimens was not determined since precipitates were too small to obtain consistent values of $\bar{b}_v$ and $\bar{b}$ by the present method. The variations of average sizes of the two sets of alloys approximately fall into straight lines in ln ($\bar{b}$) or ln ($\bar{b}_v$) vs. ln (t) plots. According to the theory of kinetics of precipitate coarsening, the growth of precipi-

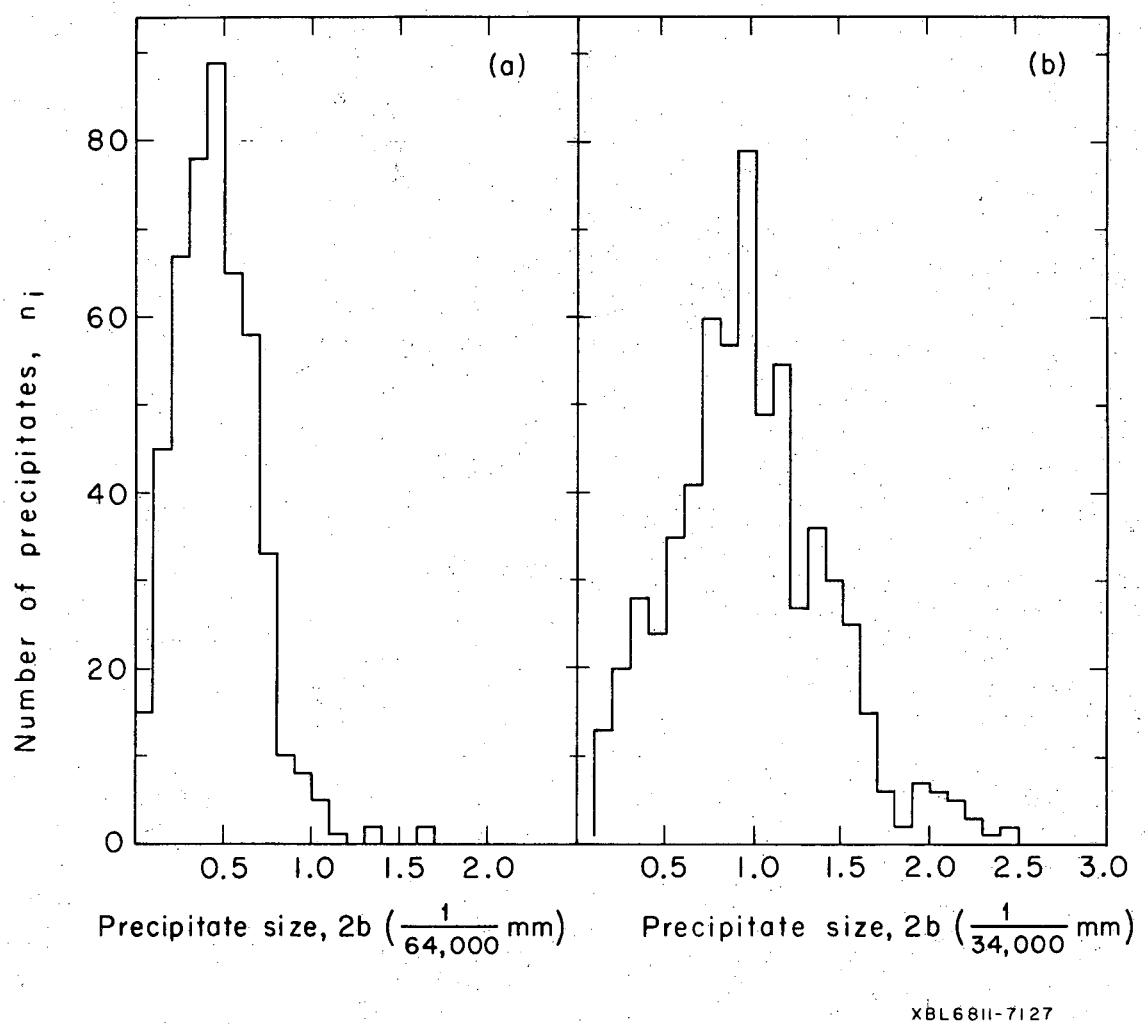

Fig. 7. Example of histograms of the number of precipitates vs precipitates sizes, (a) Alloy A aged at 1000°C for 10 hours, (b) Alloy B aged at 1000°C for 10 hours.

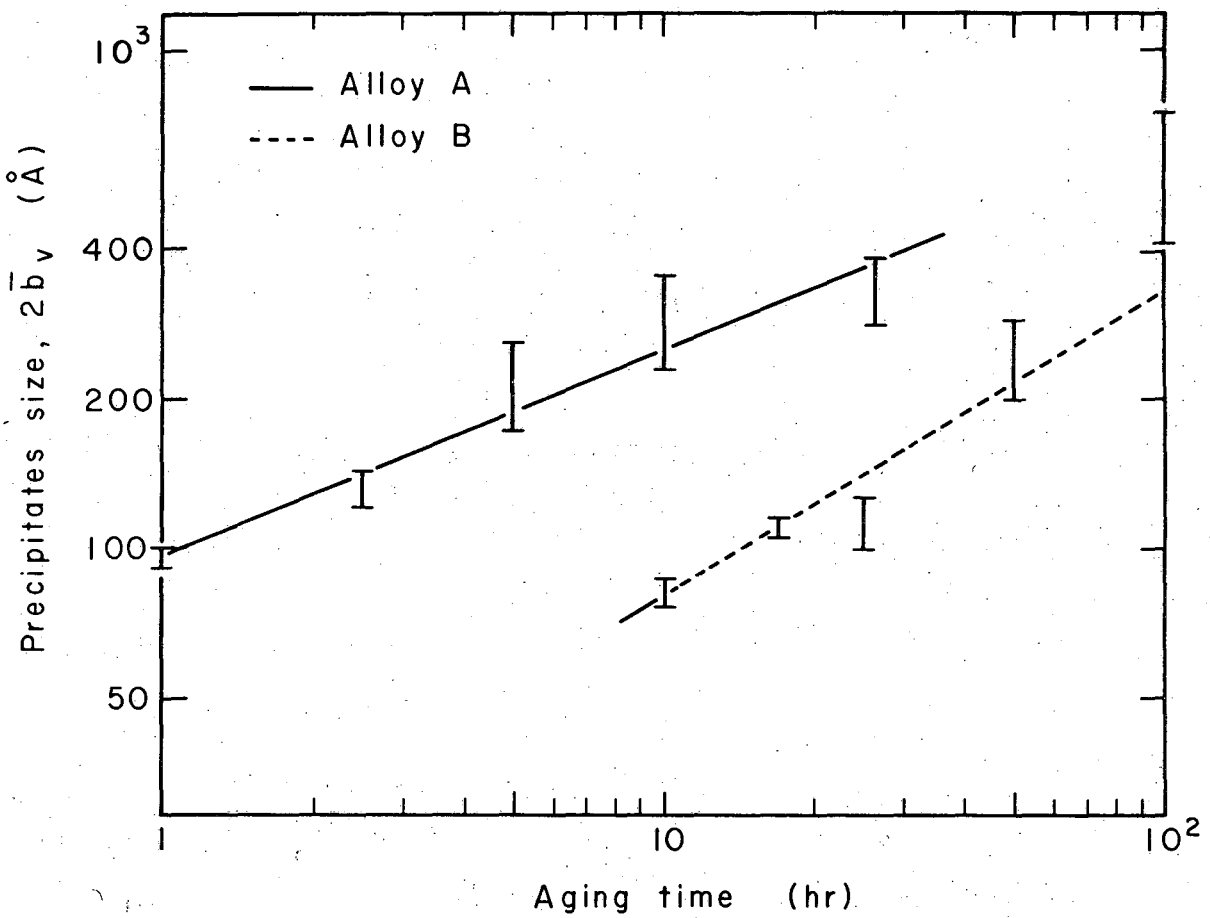

XBL6811-7126

Fig. 8. A plot of the variations of precipitates sizes with aging time.

tates with time is approximately expressed as $b(t) \simeq t^{1/3}$.[46] Hence, the slope of ln ($\bar{b}$) vs ln (t) should be 1/3. The rate of precipitate growth for the alloys A and B were faster than the rate which was expected from the theory. This is probably due to some oxygen diffusion in the aging process. This accounts for the faster rate of growth of precipitates for the alloy B than for the alloy A.

2. Determination of Interprecipitate Distances, 2δ.

The determination of average interparticle distances, 2δ is a more difficult task than that of the average sizes since it is almost impossible to make any sort of histograms of distances. Therefore, the approach was again a simple one, i.e. numbers of precipitates in a given area were counted. These were then divided by the volume (the area times average precipitates size, $2\bar{b}$). This gives the number of precipitates per unit volume, N_p, and 2δ is given by $(1/N_p)^{1/3}$. This method, in effect, assumes a cubic array of precipitates of constant size. In reality, the distribution of the precipitates is far from such an idealized form. However, the method is simple and will probably give reasonable measurements of the interprecipitates distances.

As it was shown in Fig. 6 unfortunately the distribution of the precipitates is not always uniform from one to another at magnifications which have been employed. This fact requires that counting of precipitates has to be taken from several areas of micrographs for each specimen to determine the average distance. The results of such measurements are shown in Fig. 9, with ranges of distance variations. These results indicate that nucleation of precipitates has occurred during the quenching operation and that the growth of the precipitate was by larger precipitate consuming smaller ones.

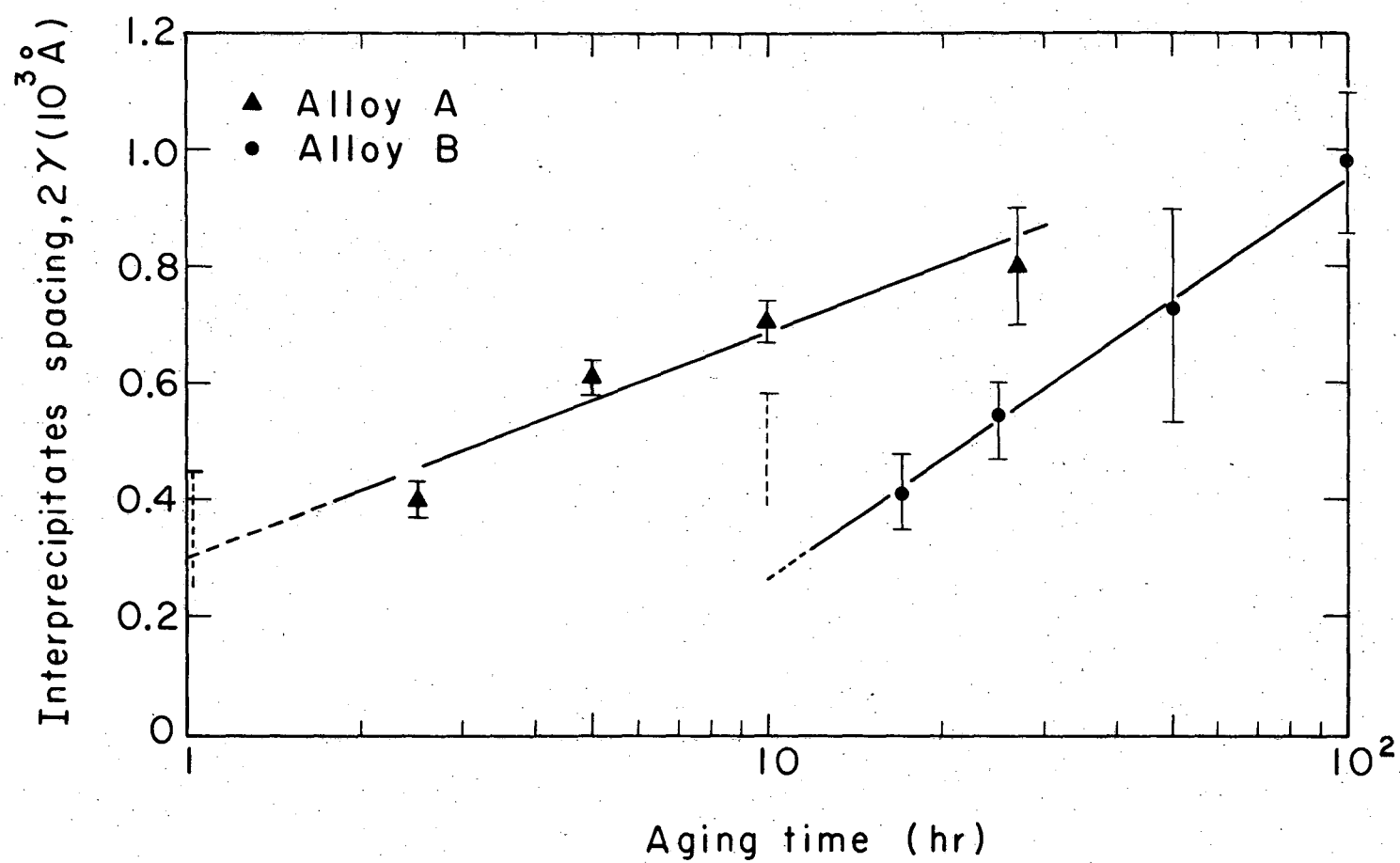

XBL6811-7125

Fig. 9 A plot of the variations of interprecipitates spacing with aging time.

IV. DISCUSSION

In Section II, we derived a relationship between critical current densities and metallurgical variables. These theoretical expressions for $J_c(H)$ have been compared with the experimental results, and the correlation of the theory with experimental results is discussed in this section.

In order to make such a comparison, we must first examine the validity of the assumptions which were used in deriving the expressions for $J_c(H)$. The major assumptions were the following: (1) The flux line - flux line interactions are weak with respect to the strength of the flux line - precipitates interaction. (2) The number of flux lines per unit area n_ϕ, is equal to or less than that of precipitates per unit area, n_p.

To check the validity of the first assumption approximate calculations of the relative energies of the interactions - flux line - flux line and flux line - precipitate interactions must be made. In order to make calculation of the flux line - flux line interaction energy an approximate expression of the interaction energy for high κ materials was used. The interaction energy of two flux lines separated by a distance r, is[23]

$$u(r) = 1/2 \left(\frac{\phi_o}{2\pi\lambda}\right)^2 K_o\left(\frac{r}{\lambda}\right)$$

where K_o is the zero order Bessel function of an imaginary argument. The values of r for applied magnetic fields at 2 and 4 kG are approximately 10^3Å and 710Å, respectively. For λ we take a value 500Å (see Table III in Appendix). Then the interaction energy is approximately 2×10^{-6} and 5×10^{-6} G^2 - cm^2. These are compared with the pinning energy per unit length, $F_p/2\delta \cong (1/n_p)^{1/2}$ and $d_{\phi_o} \cong (1/n_{\phi_o})^{1/2}$ where d_{ϕ_o} is the interflux line distance. The respective value of np and n_{ϕ_o} can be studied

comparing 2δ and d_{ϕ_o}. As mentioned above, d_{ϕ_o} is 10^3Å at H = 2 kG and 710Å at H = 4 kG. The values of 2δ vary from 400Å to 1000Å. Therefore, the assumption $n_{\phi_o} \lesssim n_p$ is well justified. Also, in the calculation of the pinning energy, it was assumed that $b \leq \xi$. To check the validity of such approximation, values of ξ are calculated with other superconducting parameter in Appendix. Such a study indicates that the approximation, $b \leq \xi$, is valid for all the alloys.

Finally, the conditions for the limiting expressions for $J_c(H)$, Eq. 15a and b, were studied to determine which expressions should be compared with the experimental results. It was observed that the ratio of the precipitate sizes to the interprecipitate spacings for all specimen was much larger than 2. Thus it follows that $\delta/R \ll 1$ and the limiting expressions for $J_c(H)$, Eq. (15b), are more appropriate. In the following the variations of J_c with the applied fields, H, is studied with reference to Eq. 15b. The dependence of J_c on the precipitates sizes and the interprecipitates spacings are then discussed.

To make a comparison of experimental and theoretical plots of $J_c(H)$ vs. H, we replot the data in J_c vs h where h is H/H_{c_2}. Then the theoretical plot, $J_c \propto \frac{1-h}{h}$ was compared with the J_c vs h curves of the heat treated alloys. Since the multiplicity factor, m, in the expression of $J_c(H)$ is unknown, only variations of J_c with h could be compared. This was done by fitting the $\frac{1-h}{h}$ curve on the experimental curves (instead of comparing with exact valves of $J_c(h)$). Representative examples of such plots are shown in Fig. 10, where agreement between the experimental and the theoretical curves are shown to be best for specimens with intermediate pinning strength specimen B ages for 25 hours. The poor agreement observed for the very weak pinning specimens (specimen B as quenched) was probably due to "peak effect." At low fields the agreement is rea-

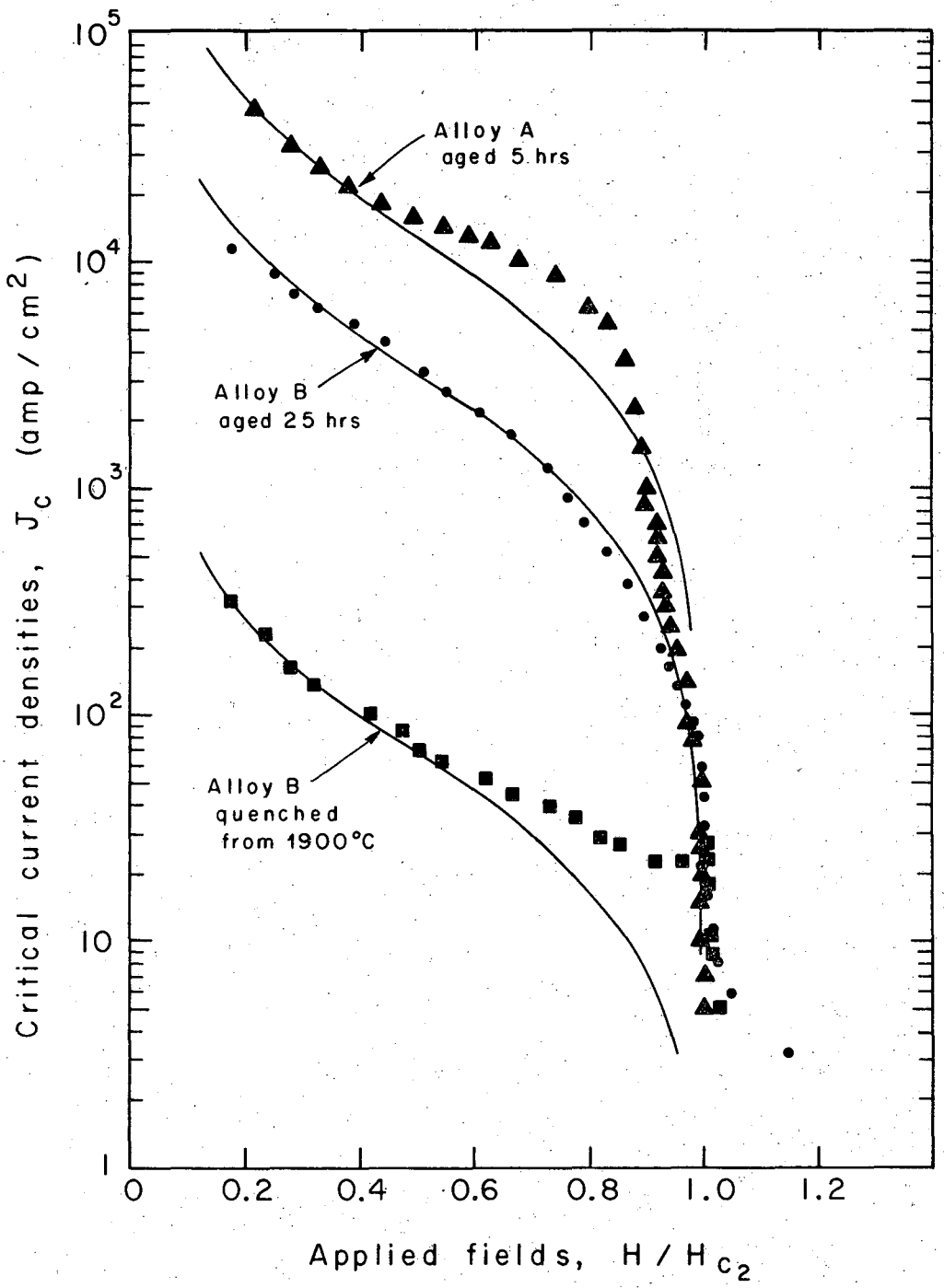

XBL6811-7124

Fig. 10 Comparison of the experimental Jc vs H curves with Eq. (15b).

sonably good, but as the applied field is increased, the interaction force among flux lines becomes stronger than the pinning from the particles. The critical current densities for weak pinning samples at higher fields are mainly controlled by the flux line-flux lattice interactions and such interaction is probably responsible for "peak effect." The effect of this is to cause an increasing deviation of the experimental points from the theoretical curve as the field strength is increased.

As the pinning of flux lines by precipitates becomes very effective, the agreement between the experimental and theoretical curves again becomes increasingly poor at higher field strength. It is recalled that one of the main assumptions in obtaining an expression for the pinning energy was to approximate the magnetization behavior of our superconducting specimens as reversible. However, the magnetization of high critical current superconductors is irreversible, and a departure of the magnetization from the reversible one is more pronounced when pinning becomes more effective. Therefore, the approximation of reversible magnetization becomes increasingly poor as the critical current density increases. This causes an increasing departure of experimental points from the theoretical curve.

Although the theoretical analysis could not account for variations of $J_c(H)$ for all ranges of pinning strength, the agreements between Eq. 15b and $J_c(H)$ curves for specimens with intermediate pinning strengths were very good in spite of the simplicity of the derivation of Eq. 15b. In order to obtain better expressions for $J_c(H)$ in the cases of extreme pinning strengths (very strong or weak), more detailed investigations would be necessary, but these investigations are beyond the scope of the present study.

In order to compare the experimental results of critical current densities of precipitate sizes and spacings variations with the theoreti-

cal results, Eq. 15b, $\frac{J_c(H)}{b^{3/2}}$ at constant fields was plotted against the interprecipitates spacing, 2δ, for alloys A and B, (Fig. 11). Although J_c depends on H_{c_2} and κ as well as b and δ, the factor $\frac{1}{H} \cdot \frac{(H_{c_2} - H)^{1/2}}{(2\kappa^2 - 1)^{1/2}}$ in the expression of $J_c(H)$ was not included in plotting the experimental results, $\frac{J_c}{b^{3/2}}$ vs δ. As it was discussed above, the expression for $J_c(H)$ accounted only for the variation of J_c with H, for some range of pinning strength. Also, in comparison with the variation of b and δ the factor $\frac{(H_{c_2} - H)^{1/2}}{H} (2\kappa^2 - 1)^{-1/2}$ does not vary appreciably from specimen to specimen for field with which we were concerned. Therefore, it was thought that the plot, $\ln \frac{J_c(H)}{b^{3/2}}$ vs $\ln \delta$ would be the best form of presenting the experimental results for comparison with Eq. 15b.

From the expression 15b, one expects the slope of $\ln J_c/b^{3/2}$ vs $\ln \delta$ to be -3/2. Lines with a slope of -3/2 are drawn through the experimental points as is shown in Fig. 11. The difference in the values of $J_c/b^{3/2}$ for the two sets of alloys is probably due to the smaller grain sizes and the presence of some large undissolved precipitates in the homogenizing process for the alloy A.

It is possible to draw lines with other slopes between -1 and -2 through the experimental points, but a line with the -3/2 slope seems to fit the data as well as any other line would. Hence, it is concluded that the experimental results are reasonably consistent with the theory in spite of the somewhat crude method which was used in measuring the interprecipitates spacings.

Furthermore, it is instructive to observe the slopes of $\ln J_c/b^3$ vs $\ln \delta$. The slopes turned out to be $\gtrsim -4$ which is much larger than the slope (-2) which would be expected from Eq. 15a. This result confirms that the choice of the limit, $\delta/R \ll 1$, was a valid choice and that the volume dependence on $J_c(H)$ was properly accounted for in the theory. Hence, it seems that

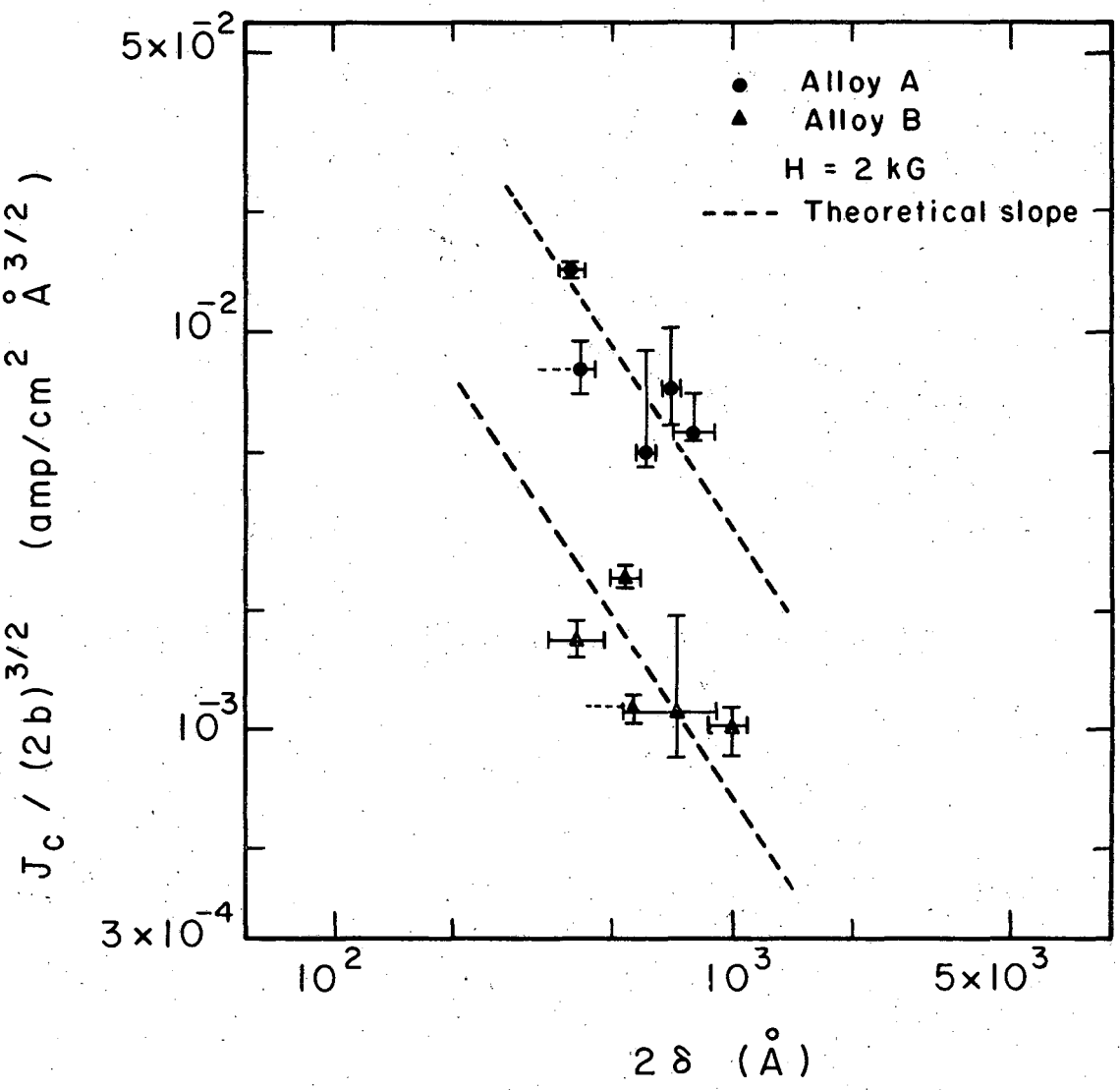

XBL6811-7123

Fig. 11 Plots of $Jc/b^{3/2}$ vs $\Delta\delta$ for the alloy A and B.

Eq. (15b) provides a proper variation of J_c with the volume of precipitates. Furthermore, we can conclude that the simple model developed can reasonably account for variations of $J_c(H)$ with precipitates changes in spacings and sizes within the approximations of the model.

Friedel et al.[35] and Coffey[26] derived expressions for the critical current densities dependence on the interprecipitates spacings. However, it was not possible to make meaningful comparison between our experimental results and their predictions. κ value for the present alloys were much too small to apply their theories. Also, their expressions do not give the explicit precipitate volume dependence for J_c. As it was discussed above, the sizes of precipitates are very critical in controlling the value of critical current densities. Thus, it is difficult to study the interparticle spacing effect on J_c without knowing the volume dependence. For this reason we did not make attempts to compare their theory and our experimental results.

V. SUMMARY

A model for flux pinning by non-superconducting precipitates has been developed: This model was compared with experimental results of the heat treated Nb 1% Zr alloys with regard to critical current densities and microstructural variations of the alloys.

1). The model developed predicts that critical current densities vary with applied fields as $J_c(H) \sim \frac{H_{c2} - H}{H}$. Experimental results showed that such variation of J_c with H was in a good agreement for alloys with intermediate pinning strength. However, the agreement became poorer for alloys with much stronger or very weak pinning strength. Those discrepancies were thought to be due to the effects which were not accounted for in the simplified model.

2). The model also predicted that critical current densities vary with precipitates size, 2b, and interparticle spacings, 2δ as $J_c \sim \left(\frac{b}{\delta}\right)^{3/2}$. The experimental results were plotted as $\ln J_c/b^{3/2}$ vs $\ln \delta$. It was observed that slopes of the plots were approximately -3/2. Although it was difficult to determine the exact slopes of $\ln J_c/b^{3/2}$ vs $\ln \delta$ plots due to the scattering of experimental points, the experimental results and the model were in accord in spite of simplifying assumptions made in developing the model.

ACKNOWLEDGEMENTS

The author wishes to express his appreciations to Professor Earl R. Parker and Professor Victor F. Zackay for their supervision of this work throught the course of this investigation. The author also wishes to express his gratitude to Dr. Robert H. Hammond, Professor Kenneth M. Ralls and Professor Marvin L. Cohen for their helpful discussions. Much appreciation is also extended to Mr. Paul R. Okamoto and Dr. Michael S. Yokota for their helpful assistance in electron microscopy.

This work was supported by the United States Atomic Energy Commission.

APPENDIX

Calculations of the coherence length, the penetration depth, and the Ginzburg-Landau parameter.

The magnetic properties of a Type II superconductor are characterized by two lengths - the coherence length, ξ, and the penetration depth, λ - and by the Ginzburg-Landau parameter, κ. In this section we calculate these parameters following B. B. Goodman's[47] simplification of the microscopic theory.[48,49]

According to this simplification, three parameters can be expressed as follows:

$$\xi(t) = \frac{0.522\xi_o}{[(1-t)\langle 1+0.752\,(\xi_o/\ell)\rangle]^{1/2}} \qquad \text{(A-1)}$$

$$\lambda(t) = \lambda(0)\,\frac{1+0.752\,(\xi_o/\ell)}{2(1-t)}^{1/2} \qquad \text{(A-2)}$$

$$\left[\begin{aligned} \kappa &= \frac{\lambda}{\sqrt{2}\xi} = \kappa_o + 7.5\times 10^{-6}\,\rho_n\delta^{1/2} \\ &= 0.96 \times \frac{L(0)}{\xi_o} + 7.5\times 10^{-6}\,\rho_n\delta^{1/2} \end{aligned}\right. \qquad \text{(A-3)}$$

where ξ_o is the B.C.S. coherence length[50] and is given by

$$\xi_o = 0.18\, \tau_r\, \sigma_F\, (\kappa_B T_c)^{-1} \cong 7.93 \times 10^{-17}\, n^{2/3}\, (S/S_F)\, (\gamma T_c)^{-1}$$

and where $\lambda_L(0)$ is the London low field penetration depth which is given by[47]

$$\lambda_L(0) = \frac{3\, ch}{\epsilon\, \kappa\, S} (\pi\gamma)^{1/2} \qquad \text{(A-5)}$$

Also, ℓ is the mean free path of an electron in the alloy, t is the ratio of the experimental temperature to the critical temperature, γ the electronic specific heat constant, S_F the velocity of an electron at the Fermi surface, S the free area of the Fermi surface in momentum space, and S_F the area of the Fermi surface for a free electron gas of denisty, n.

The value of γ was chosen as 6990 $\frac{\text{erg}}{\text{cm}^2\ \text{deg}^2}$ for all alloys. DeSorbo has shown that the value of γ is relatively constant with variation in interstitial gaseous impurity contents of Nb.[51] A plot of (Hc_2/T_c) vs ρ_n for Nb 1% Zr + O alloys also showed approximately linear dependendance of Hc_2/T_c on ρ_n in accordance with DeSorbo's result. In order to determine the value of S, the S/S_F value for Nb, 0.78,[52] is used with the value of S_F. S_F is calculated from the electron density, n, of 3.18×10^{23} $\frac{\text{elect.}}{\text{cm}^3}$. The relationship between ρ_n and ℓ is given by Pippard[53] as

$$\ell = \frac{6\, \pi^2 h}{\epsilon^2\, \rho n\, S} \qquad \text{(A-6)}$$

With the use of the values and the definitions which are described above and with the experimental value of T_c and ρ_n for the alloys in Table II. The values of ξ, λ, κ_o, and κ are calculated and tabulated in Table III.

TABLE III

Superconducting Parameters of Alloys

	Heat treatment	coherence length* $\xi(t)$	penetration depth * $\lambda(t)$	Ginzburg-Landau constant κ
ALLOY A	As quenched	1.81 10^{-6}cm	5.06 10^{-6}cm	1.98
	1.0 hr	1.89	4.93	1.85
	2.5	2.04	4.58	1.61
	5.0	2.04	4.58	1.61
	10.0	2.06	4.45	1.53
	27.0	2.10	4.42	1.49
ALLOY B	As quenched	1.77	5.30	2.12
	10 hrs	1.84	5.16	1.48
	17 hrs	1.90	4.84	1.80
	25 hrs	1.95	4.74	1.72
	50 hrs	1.48	4.68	1.67
	100 hrs	2.02	4.58	1.61

*$t \approx 0.45$

REFERENCES

1. A. A. Abrikosov, Zh. Eksperim, i Teori Fiz. 32, 1442 (1957) [English translation Soviet Phys. - JETP 5, 1174 (1957)].
2. U. Essmann and H. Trauble, Physics Letter 24 A 526 (1967). N. V. Sarma, Phys. Lett. 25A 315 (1967), H. Trauble and U. Essmann, Jour. Appl. Phys. 39 4052 (1968).
3. There have been considerable discussions on the nature of voltage drop related to flux motion. For instance, see: P.W. Anderson and Y. B. Kim, Rev. Mod. Phys. 36, 39 (1964), Y. B. Kim, C. F. Hempstead, and A. R. Strand, Phys. Rev. 139 A 1163 (1965) and P. Nozieres and W. F. Vinen, Phil. Mag. 14 667 (1966).
4. For summary see: J. D. Livingstone and H. W. Shadler, Prog. of Mat. Sci. 12 183 (1964).
5. J. B. Vetrano and R. W. Boom, J.A.P. 36 1179 (1965).
6. D. Kramer and C. G. Rhode, Trans.TMS-AIME 233, 192 (1965).
7. H. B. Shukovsky, K. M. Ralls, and R. M. Rose, Tran. TMS AIME 233, 1825 (1965). F. W. Reuter, K. M. Ralls and J. Wulff, Tran. TMS AIME 236 1143 (1966).
8. T.H. Alden and J. D. Livingstone, Appl. Phys. Letters 8, 6 (1966).
9. J. D. Livingstone, Appl. Phys. Letters 8, 319 (1966).
10. M. S. Walker, R. Stickler, and F.E. Werner, Westinghouse Research Lab. Report 62-141-448-P2 (1962).
11. E. Nembach, Phys. Stat. Sol. 13 543 (1966).
12. M. Suenaga, J. L. O'Brien, V. F. Zackay and K. M. Ralls, Trans. AIME 239 992 (1967).

13. J. S. Willis, J. F. Schenck, and R. W. Shaw, Appl. Phys. Letters 10, 101 (1967).

14. T. H. Alden and J. D. Livingstone, Jour. Appl. Phys. 37, 3551 (1966).

15. T. Doi, F. Ishida, U. Kawabe, and M. Kitada, Trans. of AIME, 242 1793 (1968).

16. A. M. Campbell, J. E. Evetts and D. Dew-Hughes, Phil Mag. 18 373 (1968).

17. E. Orowan, Symp. on Internal Stresses, p.451 Inst. of Metals, London (1948).

18. E. Orowan, Dislocations in Metals, p.131 Am. Inst. of Min. Metall. Engin. New York (1954).

19. B. B. Goodman and J. Matricon, Jour. de Phys. 27, C3-39 (1966).

20. F. Castsels, ATB Metal. 5, 19 (1964).

21. W. I. Pollock, Metals Engin. Quarterly 2, 58 (1963).

22. W. DeSorbo, Phys. Rev. 132 107 (1963).

23. P. G. DeGennes, "Superconductivity of Metal and Alloys," W. A. Benjamin Inc. New York, 1966.

24. J. E. Evetts, A. M. Campbell and Dew-Hughes, J. Phys. Chem. 1, 715 (1968).

25. J. Friedel, P. G. DeGennes, and J. Matricon, Appl. Phys. Letters 2, 119 (1963).

26. H. T. Coffey, Phys. Rev. 166 447 (1968).

27. L. Newmann and L. Tewordt, Zeit. fur Physik 189 55, (1966).

28. P. Tholfsen and Hans Meissner, Phys. Rev. 169 413 (1968).

29. E. M. Grabe and R. J. Van Thynes, "Columbium Metallurgy" Interscience Publishers, p. 139 (1961).

30. R. D. Reiswig, Trans. of AIME 230, 914 (1964).

31. D. O. Hobson, "Aging Phenomena in Columbium-Base Alloys" presented at the AIME High-Temperature Material Conference, Cleveland, Ohio, April, 1961.

32. A. C. Barber and P. A. Morton, "High Temperature Refractory Metals" Metallurgical Society Conference V. 34, p.391 (1964), Gordon and Breach Science Publishers, Inc., New York.

33. M. E. Merriam and M. van Hergen, Phys. Rev. 131, 637 (1963).

34. V. L. Ginzburg and L. D. Landau, Zh. Eksperim i Teor. Fiz. 20, 1064 (1950).

35. P. L. Gor' kov, Zh Eksperim i Teor. Fiz. 37, 835, 1407 (1959).

36. Om Johari, Metals 20, 26 (1968).

37. P. B. Hirsch, A. Howie, R. B. Nicholson, and D. W. Pashley, and M. J. Whelan "Electron Microscopy of Thin Crystals" p. 415, Butterworths, London 1965.

38. G. Thomas, "Transmission Electron Microscopy of Metals", John Wiley and Sons, Inc., New York, 1962.

39. R. D. Heidenreich, "Fundamentals of Transmission Electron Microscopy", Interscience Publishers, New York, 1964.

40. R. D. Heidenreich and C. J. Calbrick, Electron Microscopy in "Physical Methods of Chemical Analysis" Vol. 1 - - 2nd Edition, ed. W. G. Beck, Academic Press, New York (1960).

41. R. B. Fischer, Electron Mettalography, Sym. on Techniques, Am. Soc. Testing Materials Spec. Tech. Publ. No. 155 (1953).

42. J. van Landuyt, Phys. Stat. Sol. 6, 957 (1964).

43. R. L. Fullman, Trans. AIME 197, 447 (1953).

44. C. S. Smith and L. G. Utterman, Trans. AIME 197, 81 (1953).

45. R. T. De Hoff, Trans. AIME 233, 25 (1965).

46. M. E. Fine, "Introduction to Phase Transformations in Condensed Systems", p. 68, Macmillan Company, New York (1964); I. M. Lifshitz and W. W. Slyozov, J. Phys. Chem. Solids 19, 35 (1961); J. S. Hirshborn, Metal Science Jour. 1, 91 (1967).

47. B. B. Goodman, Reports on Prog. in Phys. 24, 445 (1966).

48. L. P. Goikov, Zh. Eksper. Teor. Fiz. 36, 1918 (1959) (Soviet Phys. JETP 9, 1364 (1959). English Trans.) Zh Eksper. Teor. Fiz. 37, 1407 (1959) (Soviet Phys. JETP 10, 998 (1960): English Trans.)

49. C. Caroli, P. G. de Gennes, and J. Matricon, Phys. Kondens. Materie, 1, 176 (1963).

50. J. Bardeen, L. N. Cooper, and R. Schrieffer, Phys. Rev., 108, 1175 (1957).

51. W. De Sorbo, Phys. Rev., 132, 107 (1963).

52. T. F. Stromberg and C. A. Swanson, Bull. Am. Phys. Soc., 10, 358 (1965).

53. A. B. Pippard, Repts. on Progr. in Phys. 23, 191 (1960).

FIGURE CAPTIONS

1. a) A diagram showing the respective orientation of magnetic fields, H, and currents, J, through a specimen.

   b) A schematic diagram of a flux line which is pinned by precipitates.

2. Plots of critical current densities vs. applied fields for the alloys A and B.

3a. Optical micrographs of the alloys

   (a) as quenched from 1800°C, and aged at 1000°C for (b) 1 hours, (c) 10 hours, and (d) 27 hours.

3b. Optical micrographs of the alloys B.

   (a) as quenched from 1900°C, and aged at 1000°C for (b) 10 hours (c) 25 hours and (d) 100 hours.

4. Transmission electron micrographs of the alloys Nb 1% Zr

   (a) as quenched from 1900°C then aged at 1000°C for (b) 10 hours and (c) 35 hours.

5a. Carbon replication micrographs of the alloys A.

   (a) as quenched from 1800°C, and aged at 1000°C for (b) 2 hours, (c) 10 hours and (d) 27 hours.

5b. Carbon replication micrographs of the alloys B.

   (a) as quenched from 1900°C, and aged at 1000°C for (b) 10 hours, (c) 25 hours and (d) 50 hours.

5c. Carbon replication micrograph of the alloy A quenched from 1800°C and aged for 1 hour at 1000°C showing details of the precipitates.

5d. Carbon replication micrograph of the alloy A quenched from 1800°C and aged for 27 hours showing details of precipitates.

6. (a) The alloy B aged at 1000°C for 50 hours. An example of replication micrographs showing variations of precipitated distributions

which are observed at different magnifications, and an electron diffraction rings from the area shown.

7. Example of histograms of the number of precipitates vs precipitates sizes, (a) Alloy A aged at 1000°C for 10 hours. (b) Alloy B aged at 1000°C for 10 hours.

8. A plot of the variations of precipitates sizes with aging time.

9. A plot of the variations of interprecipitates spacing with aging time.

10. Comparison of the experimental Jc vs H curves with Eq. (15b).

11. Plots of $Jc/b^{3/2}$ vs $\Delta\delta$ for the alloy A and B.

LEGAL NOTICE

This report was prepared as an account of Government sponsored work. Neither the United States, nor the Commission, nor any person acting on behalf of the Commission:

A. Makes any warranty or representation, expressed or implied, with respect to the accuracy, completeness, or usefulness of the information contained in this report, or that the use of any information, apparatus, method, or process disclosed in this report may not infringe privately owned rights; or

B. Assumes any liabilities with respect to the use of, or for damages resulting from the use of any information, apparatus, method, or process disclosed in this report.

As used in the above, "person acting on behalf of the Commission" includes any employee or contractor of the Commission, or employee of such contractor, to the extent that such employee or contractor of the Commission, or employee of such contractor prepares, disseminates, or provides access to, any information pursuant to his employment or contract with the Commission, or his employment with such contractor.

TECHNICAL INFORMATION DIVISION
LAWRENCE RADIATION LABORATORY
UNIVERSITY OF CALIFORNIA
BERKELEY, CALIFORNIA 94720